CSMFO Lab. http://www.tn.ifn.cnr.it/

Glass-Based
Sub-Wavelength Photonic Structures

Andrea Chiappini[1], Alessandro Chiasera[1], Anna Lukowiak[1,2], Davor Ristic[1,3], Iustyna Vasilchenko[1,4], Brigitte Boulard[5], Claire Duverger Arfuso[5], Cristina Armellini[1,6], Alessandro Carpentiero[1], Stefano Varas[1], Simone Normani[1,4], Inas K. Battisha[7], Gilles Cibiel[8], Giancarlo C. Righini[9,10], Maurizio Ferrari[1]

[1]IFN – CNR CSMFO Lab., Via alla Cascata 56/C Povo, 38123 Trento, Italy
[2]Institute of Low Temperature and Structure Research, PAS, 50-422 Wroclaw, Poland
[3]Ruđer Bošković Institute, P.O. Box 180, 10002 Zagreb, Croatia
[4]Dipartimento di Fisica, Università di Trento, via Sommarive 14, Povo, 38123 Trento, Italy
[5]IMMM, UMR 6283, Equipe Fluorures, Université du Maine, Le Mans, France
[6]FBK Center for Materials & Microsystems, Via Sommarive 18, Povo 38123 Trento, Italy
[7]National Research Center, 12622 Dokki, Giza, Egypt
[8]Centre National d'Etudes Spatiales (CNES), 31401 Toulouse Cedex 9, France
[9]IFAC - CNR, MiPLa.b, Via Madonna del Piano 10, 50019 Sesto Fiorentino, Italy
[10]Museo Storico della Fisica e Centro di Studi e Ricerche Enrico Fermi, P.zza Viminale 1, 00184 Roma, Italy

Dipartimento di Fisica Scuola di Dottorato Università di Perugia 09 aprile 2014

INSTITUTE FOR PHOTONICS AND NANOTECHNOLOGIES (IFN)

lighting the way ahead

Dipartimento di Fisica Scuola di Dottorato Università di Perugia 09 aprile 2014

OUTLINE

- Motivation of Glass Photonics Research
- Glass Ceramics
  - § Down conversion systems
  - § SnO_2 nanocrystals as sensitizers
- Photonic Crystals
  - § Opals
  - § 1D microcavities
- Spherical microresonators
- Conclusions and Perspectives

CNR DSFTM

Scienze fisiche e tecnologie della materia

Consiglio Nazionale delle Ricerche

Istituto di Fotonica e Nanotecnologie - Unità di Trento

CSMFO Lab. http://www.tn.ifn.cnr.it/

FONDAZIONE BRUNO KESSLER

MOTIVATION OF GLASS PHOTONICS RESEARCH

MOTIVATION

Light control

Nano scale confined structures

- Glass-ceramic waveguides
- Photonic crystals (n-D, Fibers)
- Colloidal systems

Micro scale confined structures

- Fibers and Waveguides
- Resonators
- Cavities

Novel materials, functionalizations, and geometries

WE START FROM:

$$I_{th} = \frac{h\nu_p}{\sigma_p \tau}$$

AND...............

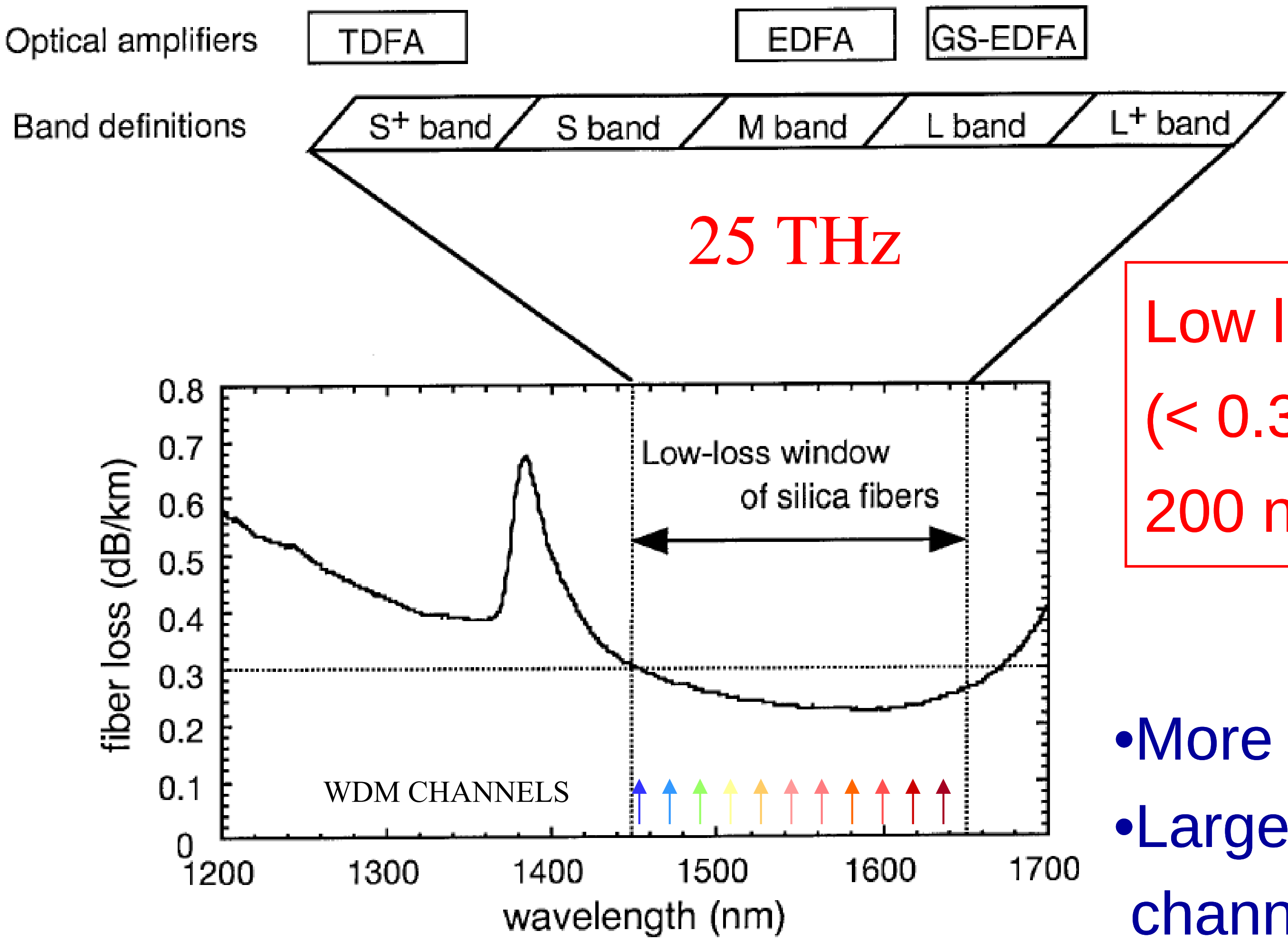

Low loss window (< 0.3 dB/Km) is 200 nm wide

- More channels
- Largely-spaced channels
- Non-zero dispersion

Range of high Gain EDFAs 4 THz

GLASS CERAMICS AND ENERGY TRANSFER

Tb^{3+} and Yb^{3+} ions in sol-gel derived SiO_2-HfO_2 glass ceramic planar waveguides

SPIE Newsroom

10.1117/2.1201105.003701

Rare-earth doped materials enhance silicon solar cell efficiency

Guillaume Alombert-Goget, Davor Ristic, Alessandro Chiasera, Stefano Varas, Maurizio Ferrari, Giancarlo C. Righini, Belto Dieudonne, and Brigitte Boulard

Down conversion with Tb^{3+}/ Yb^{3+}

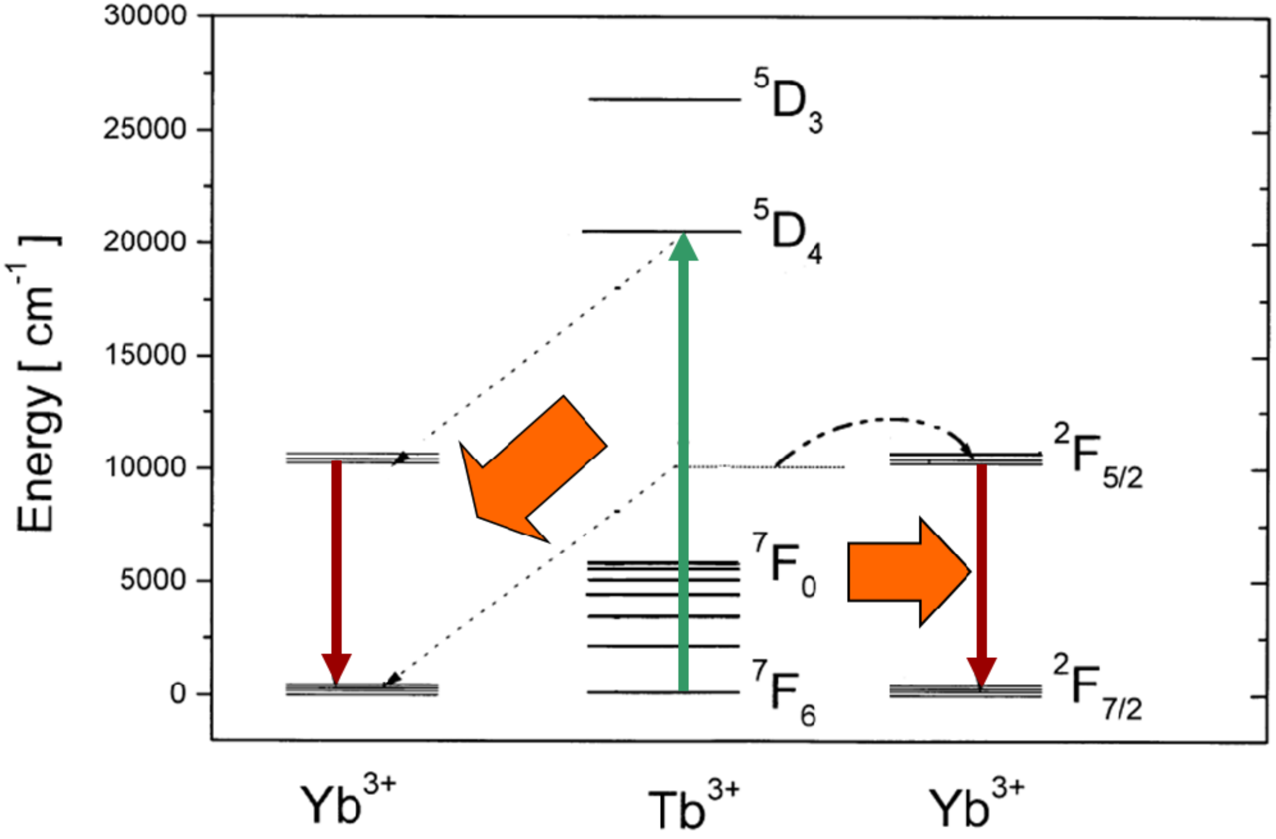

One green photon @ 488nm → **Two red photon @ 980 nm**

Down-converters Silica-Hafnia glass ceramics

- **Low phonon energy (~ 700 cm^{-1})**
- **Rare earth solubility**
- **Combine spectroscopic properties of the crystal with optical properties of the glass**

- **Determine the efficiency of the process**
- **Optimize the rare earth ions content**

Prepared waveguides

Rare earth concentration, refractive index and thickness of the waveguides

Sample label	Terbium concentration in mol%	Ytterbium concentration in mol%	n@543.5 nm TE polarization [± 0.001]	n@632.8 nm TE polarization [± 0.001]	Layer thickness [±0.2μm]
AR1	0.5	0	1.621	1.616	1.0
A1	0.5	1	1.626	1.621	1.0
A2	0.5	2	1.631	1.626	1.0
A3	0.5	3	1.633	1.628	1.1
BR1	0.2	0	1.623	1.617	1.1
B1	0.2	0.8	1.604	1.608	0.9
BR3	0.6	0	1.624	1.620	1.1
B3	0.6	2.4	1.630	1.625	1.2
BR5	1	0	1.626	1.621	1.2
B5	1	4	1.638	1.633	1.1

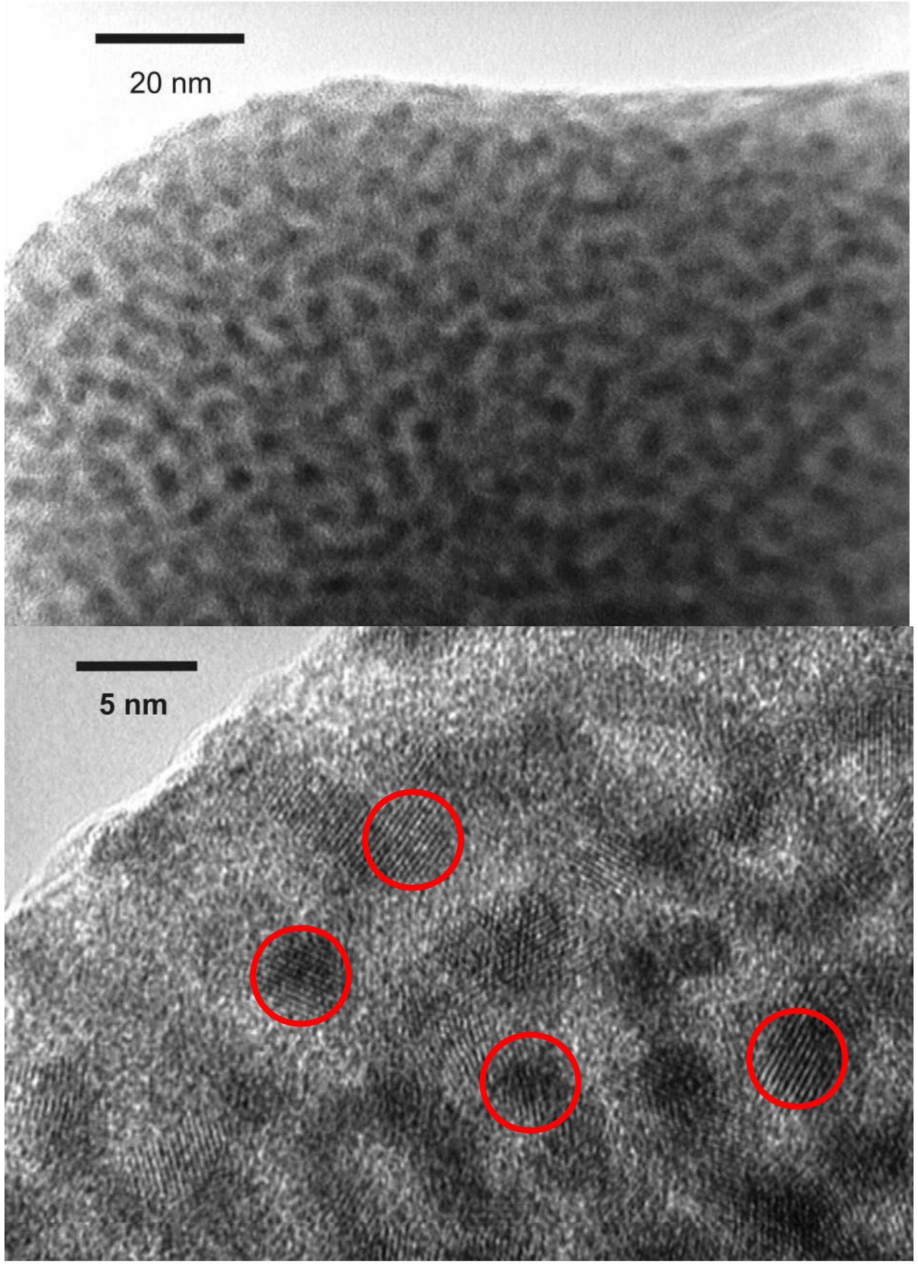

TEM images

- **Validation of the process: Incorporation of hafnia nanocrystals in the waveguide**
- **Nanocrystals identified as monoclinic HfO_2**
- **Size of about 3-4 nm**

Photoluminescence spectra

Room temperature photoluminescence spectra of the $^2F_{5/2} \rightarrow {}^2F_{7/2}$ transition of Yb^{3+} ions after excitation at 476 nm for the three samples of the first series. Each spectrum was normalized to the maximum of the luminescence intensity.
The emission of the Yb^{3+} ion after excitation at 476 nm is a indication of the presence of an **efficient energy transfer from Tb^{3+} to Yb^{3+}**.

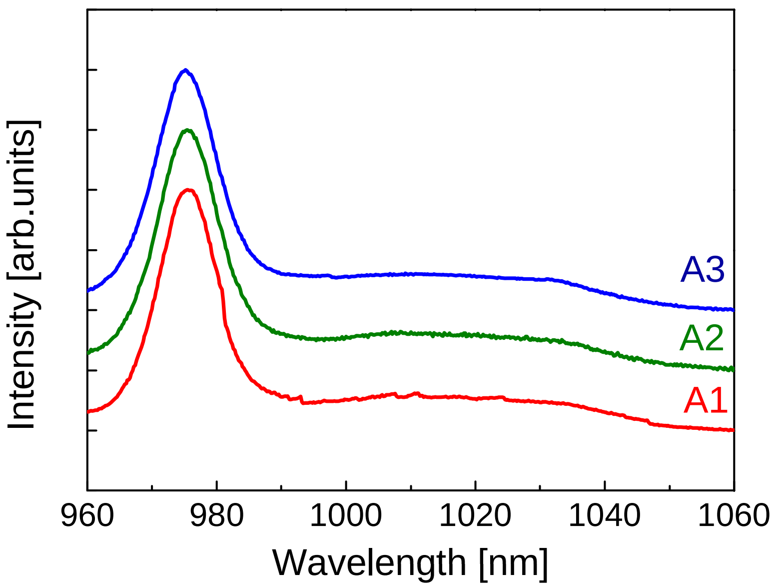

Tb 0.5 mol%

A1 1 mol% Yb

A2 2 mol% Yb

A3 3 mol% Yb

However, it is not possible to *evaluate* the conversion efficiency only on the base of the photoluminescence spectra.

The TE_0 mode waveguiding excitation was used for luminescence measurements, by detecting the light coming out from the waveguide surface. Luminescence spectroscopy was performed using the 476 nm line of an Ar^+ ion laser as excitation source at 600 mW power.

Decay curves analysis

Energy transfer efficiency between Tb^{3+} and Yb^{3+} :

$$\eta_{Tb-Yb} = 1 - \frac{\int I_{Tb-Yb}\,dt}{\int I_{Tb}\,dt}$$

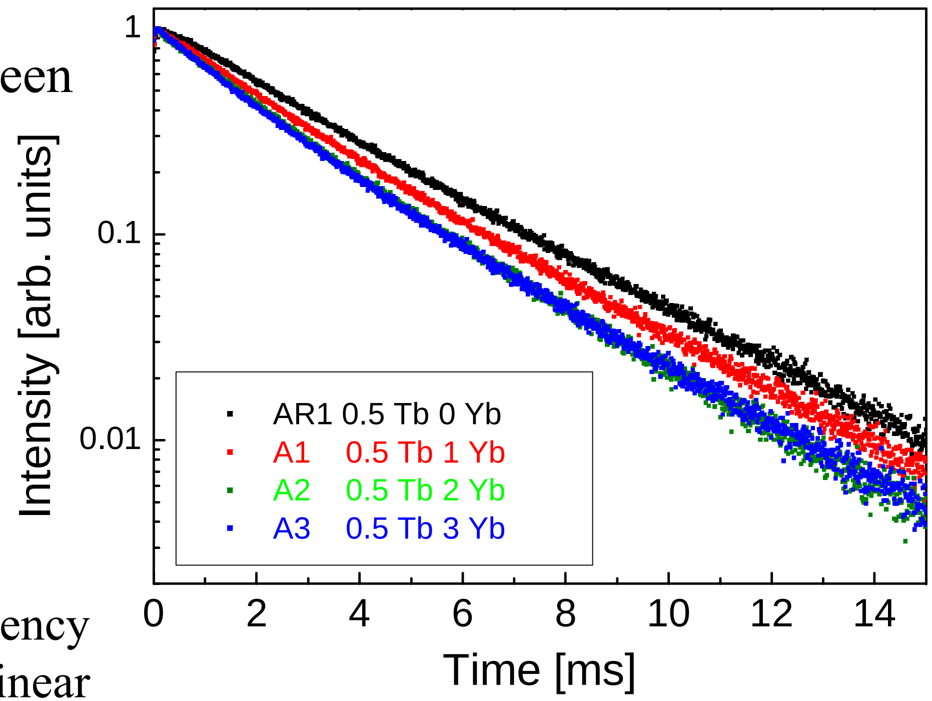

Decay curves of the luminescence from the $^5D_4$ metastable state of Tb^{3+} ions for the first samples series under excitation at 355 nm.

The relation between the transfer efficiency and the **effective quantum efficiency** is linear and is defined as:

$$\eta_{EQE} = \eta_{Tb-r}(1-\eta_{Tb-Yb})+2\eta_{Tb-Yb}$$

where the quantum efficiency for Tb^{3+} ions, η_{Tb-r}, is set equal to 1.

Tb^{3+}/ Yb^{3+} down conversion efficiency

Transfer efficiency and effective quantum efficiency as a function of Yb^{3+} molar concentration for A samples where Tb^{3+} content is fixed at 0.5 mol%

Composition (Yb concentration in mol%)	1%	2%	3%
Estimated transfer efficiency (in glass ceramic)	14%	24%	25%
Estimated effective quantum efficiency (in glass ceramic)	114%	124%	125%
Estimated transfer efficiency (in glass)	2%	4%	6%
Estimated effective quantum efficiency (in glass)	102%	104%	106%

For compositions with Tb^{3+} content kept constant at 0.5 mol% and increasing Yb^{3+} molar concentration, we observed that:

- the Tb-Yb energy transfer efficiency increases with the increase of the molar ratio Yb/Tb;
- the energy transfer efficiency does not exceed 24-25%.

SnO_2-SiO_2 Glass-Ceramic Waveguides

Heat Treatment at
900, 1000, 1100 °C for 30’- 5h

Samples:
92 SiO_2 - 8 SnO_2 : 1 mol% Eu^{3+}_HT at 800, 900, 1000, 1100°C for 30’.
84 SiO_2 - 16 SnO_2 : 1 mol% Eu^{3+}_HT at 800, 900, 1000, 1100°C for 30’.
75 SiO_2 - 25 SnO_2 : 1 mol% Eu^{3+}_HT at 800, 900, 1000, 1100°C for 30’, 1100 °C for 1h and 5h.

S.N.B. Bhaktha, F. Beclin, M. Bouazaoui, B. Capoen, A. Chiasera, M. Ferrari, C. Kinowski, G.C. Righini, O. Robbe, S. Turrell
“Enhanced fluorescence from Eu^{3+} in low-loss silica glass-ceramic waveguides with high SnO_2 content”
Applied Physics Letters 93 (2008) pp. 211904-1/3.

T.T. Van Tran, T. Si Bui, S. Turrell, B. Capoen, P. Roussel, M. Bouazaoui, M. Ferrari, O. Cristini, and C. Kinowski
“Controlled SnO_2 nanocrystal growth in SiO_2-SnO_2 glass-ceramic monoliths”
Journal of Raman Spectroscopy 43 (2012) pp. 869-875.

TEM

Homogeneous distribution

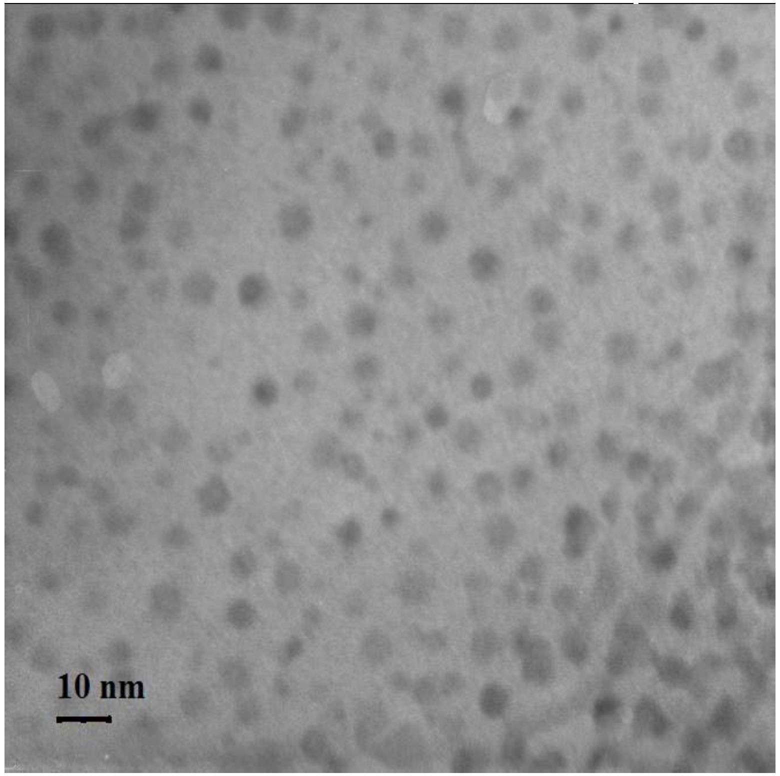

About 4 nm NCs

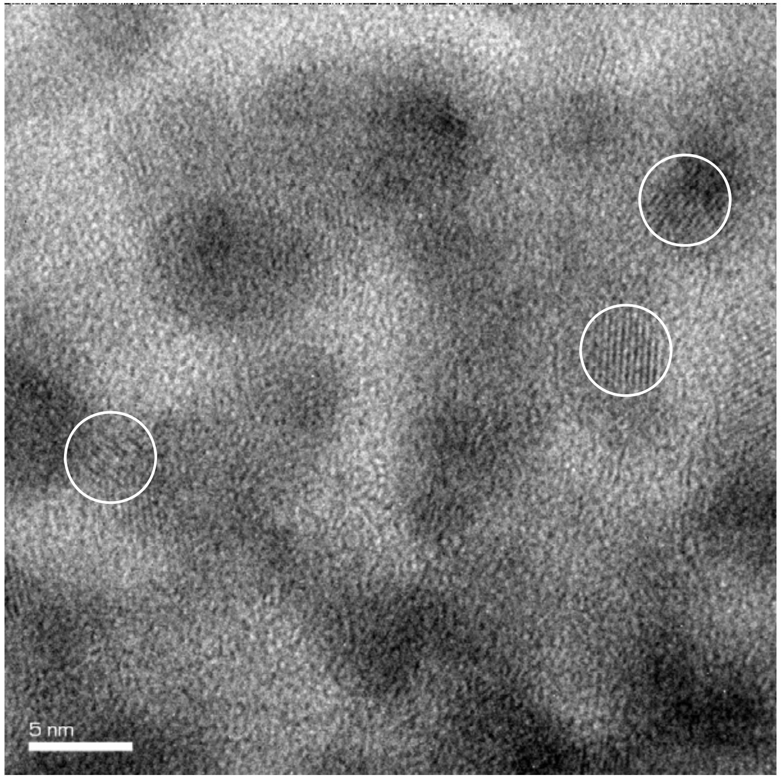

Raman spectra

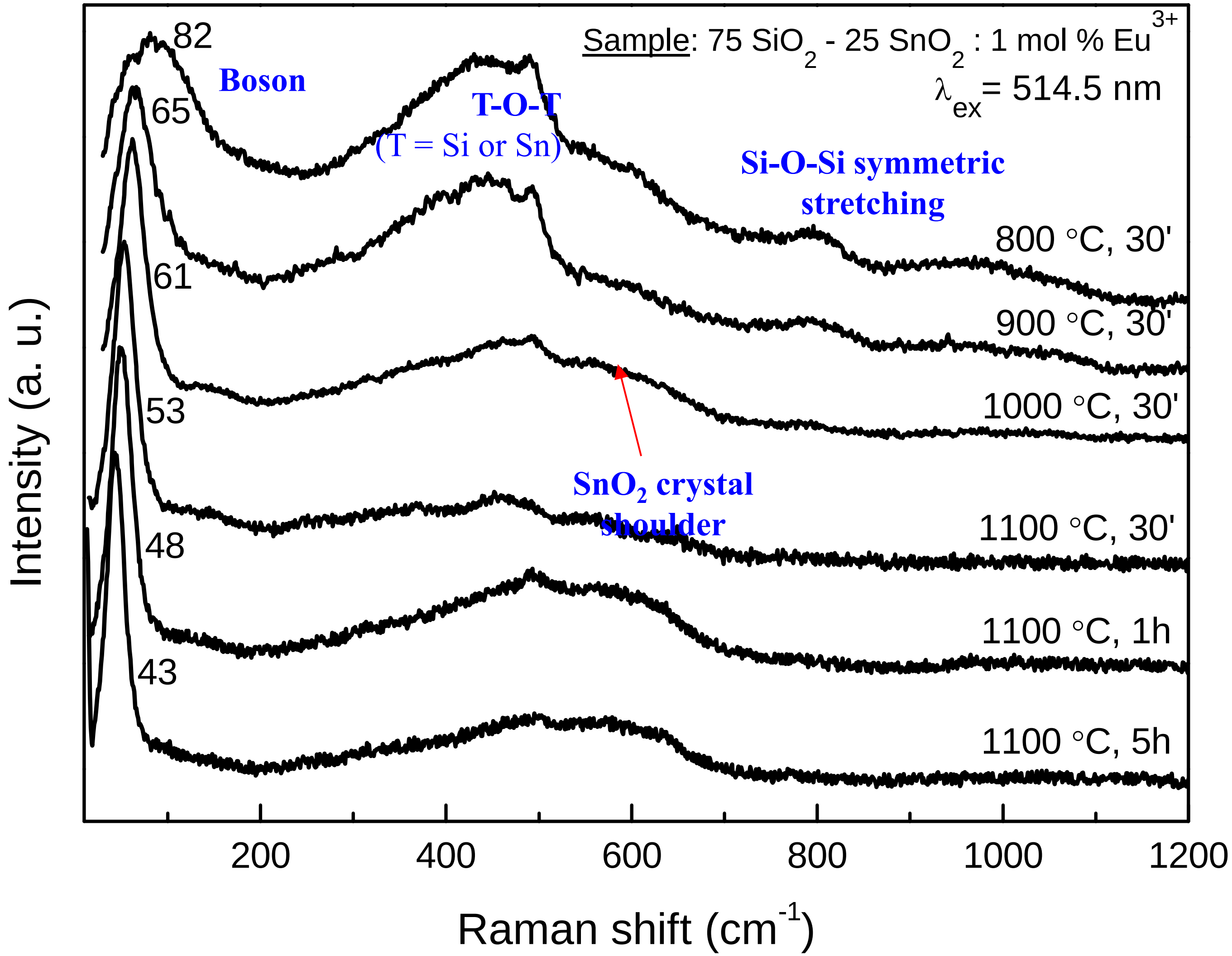

$$\omega = S_{l,n} \frac{v}{Lc}$$

ω = wavenumber
v = sound velocity
L = particle size
c = speed of light

- Crystal-peak observed in the low-frequency region.
- Increasing shoulder centered around 550 cm^{-1} is attributed to the SnO_2 crystals.

Excitation spectra

Room temperature excitation spectra of $^5D_0 \rightarrow {}^7F_2$ emission at 613 nm

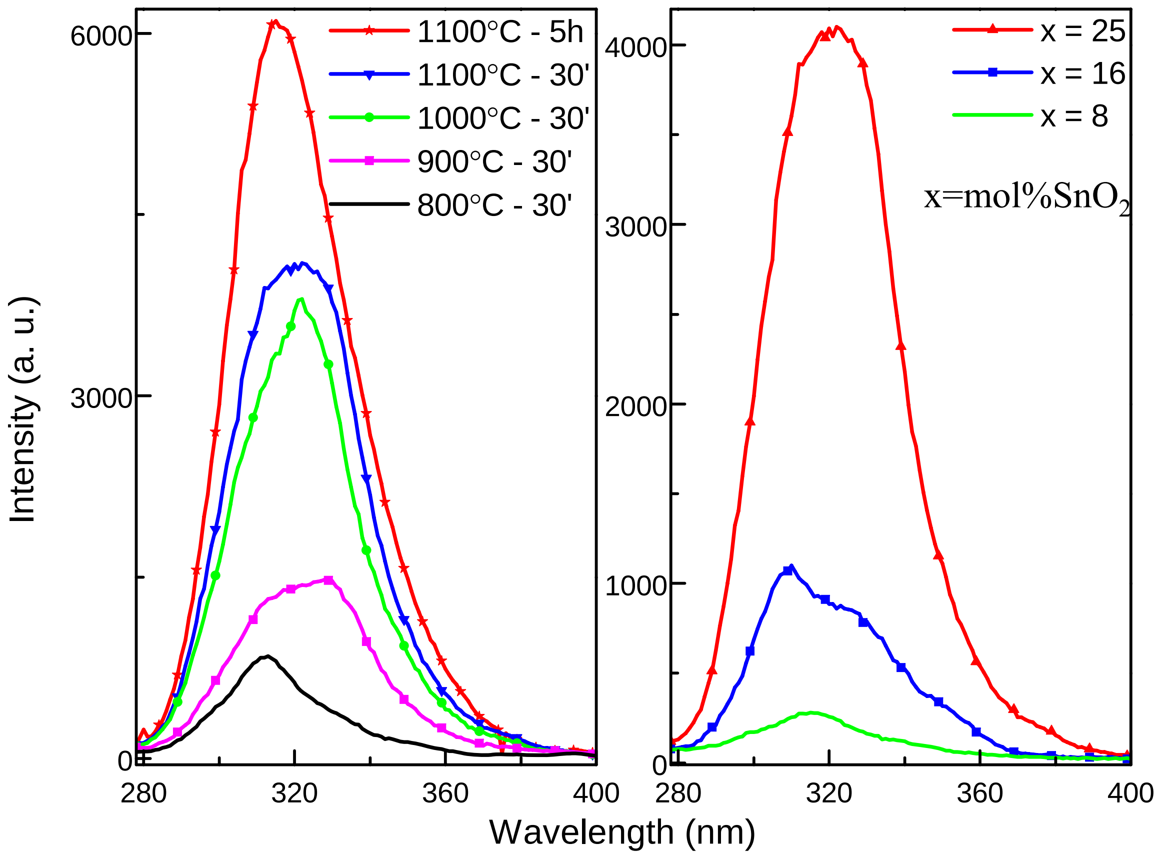

The broad and strong band observed at 310 nm (4.0 eV) corresponds to the SnO_2 band-gap energy.

PL spectra λ_{ex}=351nm

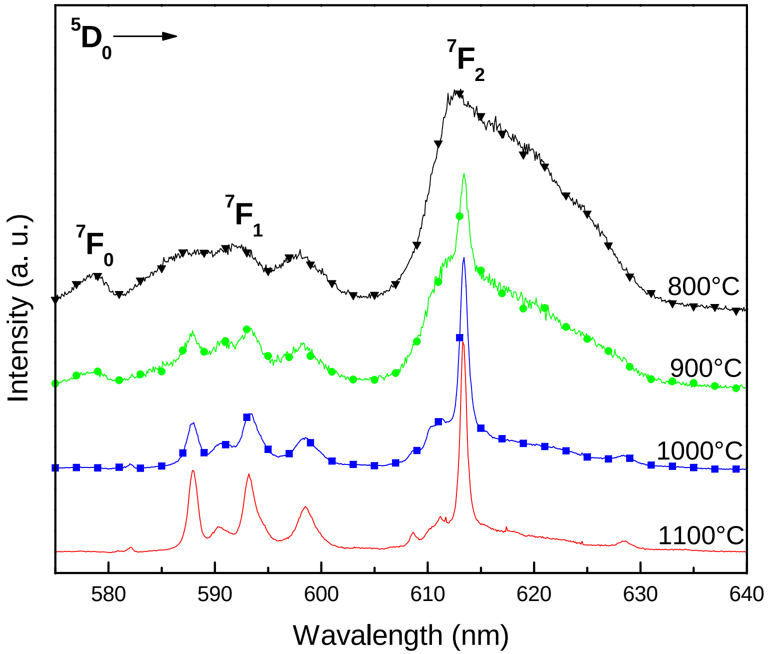

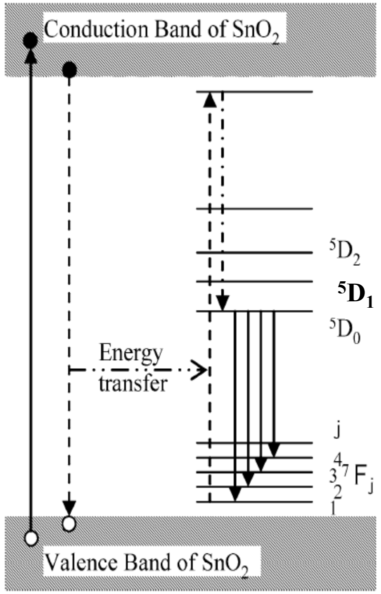

For annealing temperature higher than 900 °C the emission **features typical of Eu^{3+} ion in a crystalline like environment** are predominant, *indicating that most part of Eu^{3+} ions are embedded in SnO_2 nanocrystals*

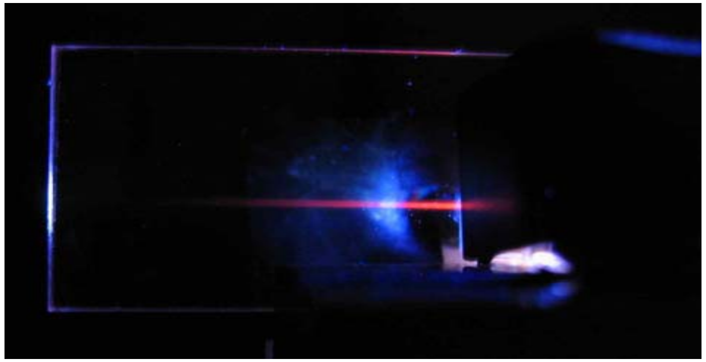

Enhanced fluorescence from Eu^{3+} in low-loss silica glass-ceramic waveguides with high SnO_2 content

λ_{ex} = 351 nm

S.N.B. Bhaktha, F. Beclin, M. Bouazaoui, B. Capoen, A. Chiasera, M. Ferrari, C. Kinowski, G.C. Righini, O. Robbe, S. Turrell, "Applied Physics Letters 93 (2008) pp. 211904-1/3.

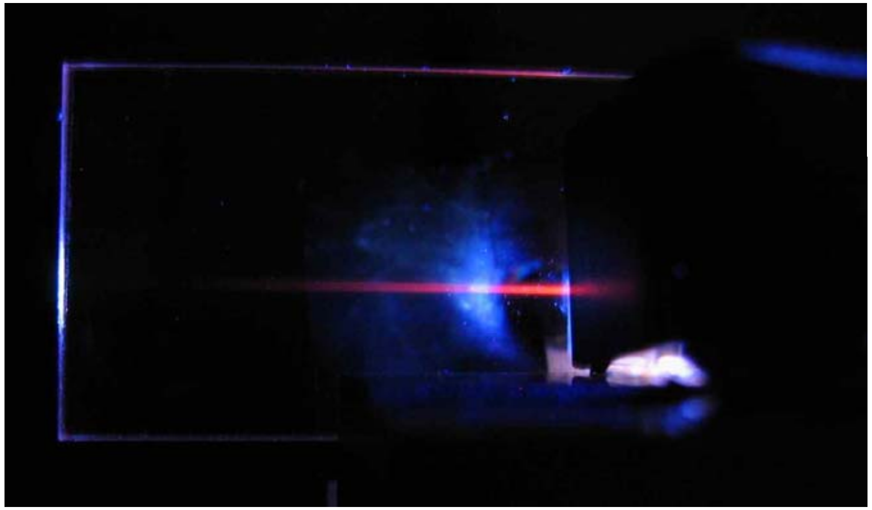

Crack-free and low loss glass ceramic waveguide $75SiO_2$-$25SnO_2$: Eu^{3+} fabricated by sol gel, dip-coating method. Losses remain below 0.8 dB/cm.

High photosensitivity in low-loss sol-gel $SiO_2 – SnO_2$ waveguides

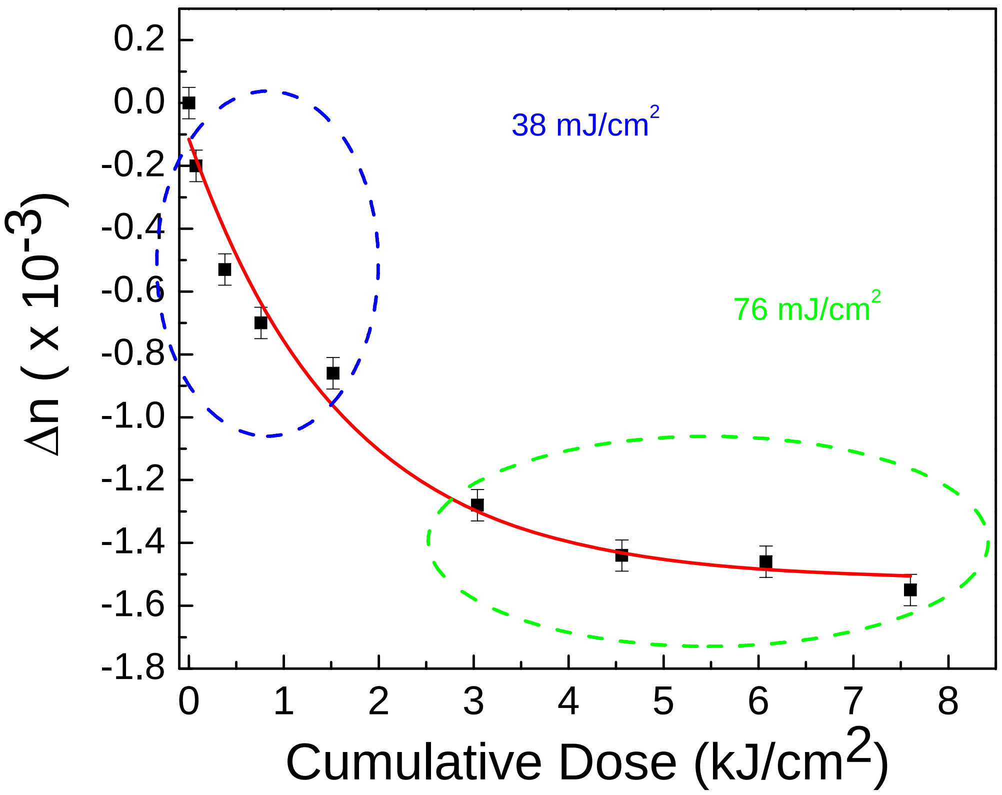

Effective index change at 1550 nm for the single mode waveguide after the UV irradiation at 248 nm as a function of cumulative doses used. The solid line is an help for the eyes.

S.Berneschi, S.N.B. Bhaktha, A. Chiappini, A. Chiasera, M. Ferrari, C. Kinowski, S. Turrell, C. Trono, M. Brenci, I. Cacciari, G. Nunzi Conti, S. Pelli, G. C. Righini "Highly photorefractive Eu^{3+} activated sol-gel $SiO_2 – SnO_2$ thin film waveguides"
Proceedings of SPIE Vol. 7604 (2010) pp. 76040Z-1/6

High photosensitivity in low-loss sol-gel $SiO_2 – SnO_2$ waveguides

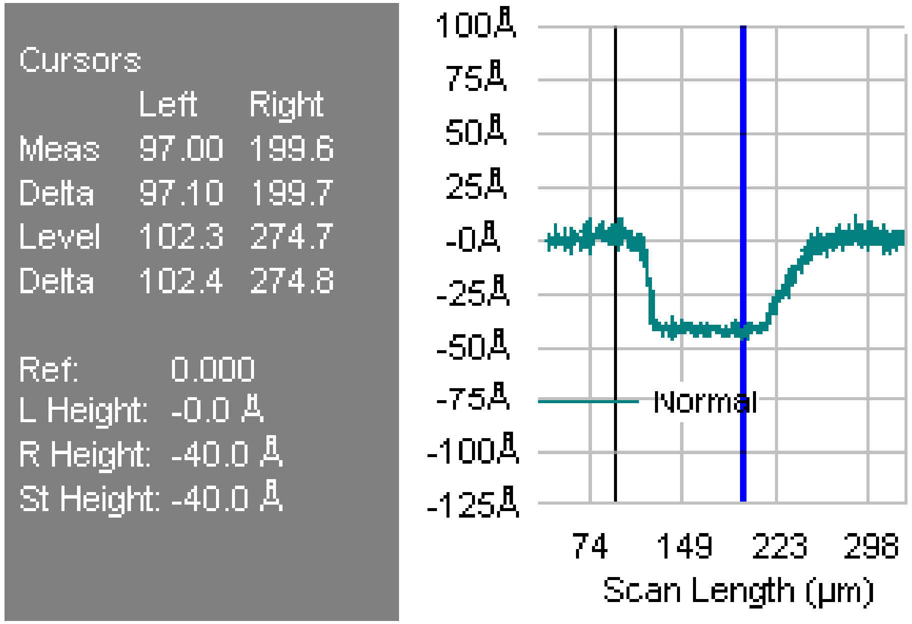

A swelling of about 4 nm was observed in UV exposed regions

B.N. Shivakiran Bhaktha, Simone Berneschi, Gualtiero Nunzi Conti, Giancarlo C. Righini, Andrea Chiappini, Alessandro Chiasera, Maurizio Ferrari, Sylvia Turrell
"Spatially localized UV-induced crystallization of SnO_2 in photorefractive SiO_2-SnO_2 thin film".
Proceedings of SPIE Vol. 7719 (2010) pp. 77191B-1/5.

S.Berneschi, S.N.B. Bhaktha, A. Chiappini, A. Chiasera, M. Ferrari, C. Kinowski, S. Turrell, C. Trono, M. Brenci, I. Cacciari, G. Nunzi Conti, S. Pelli, G. C. Righini "Highly photorefractive Eu^{3+} activated sol-gel SiO_2 – SnO_2 thin film waveguides"
Proceedings of SPIE Vol. 7604 (2010) pp. 76040Z-1/6

CNR DSFTM
Scienze fisiche e tecnologie della materia
Consiglio Nazionale delle Ricerche
Istituto di Fotonica e Nanotecnologie - Unità di Trento
CSMFO Lab. http://www.tn.ifn.cnr.it/
ifn
FONDAZIONE BRUNO KESSLER

PHOTONIC CRYSTALS

OPALS: A SUITABLE PHOTONIC STRUCTURE FOR LIGHT CONFINEMENT

Molar Concentrations

- $[TEOS] = 0.22\ M$
- $[NH_3] = 1.0\ M$
- $[H_20] = 15.0\ M$

Stober Methods

$$Si(OC_2H_5)_4 + 4H_2O \rightarrow Si(OH)_4 + 4C_2H_5OH$$

$$Si(OH)_4 \rightarrow SiO_2 + 2H_2O$$

Silica Spheres

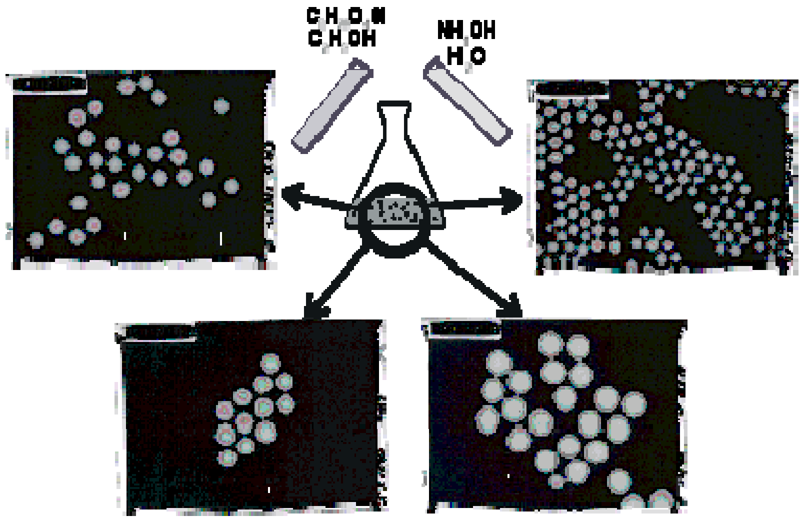

the **dimension of** :~255nm

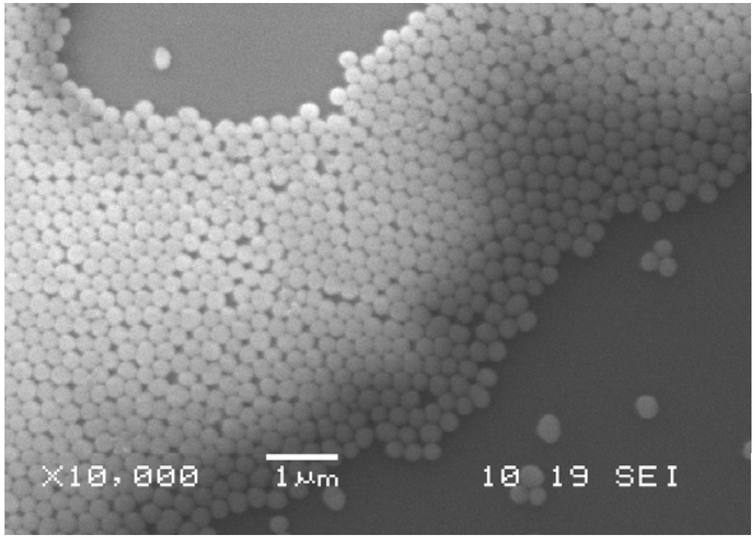

high uniformity of ***silica spheres***
(less than 5% of dispersion in diameter)

The reaction takes place at room temperature and
we can control the particle size through the concentration of a single reactive.

3D Photonic Crystals bottom-up approach

Self-Assembling
colloidal nano-microspheres

Low cost

associated with their manufacture

"Easy"

relative easiness of preparation

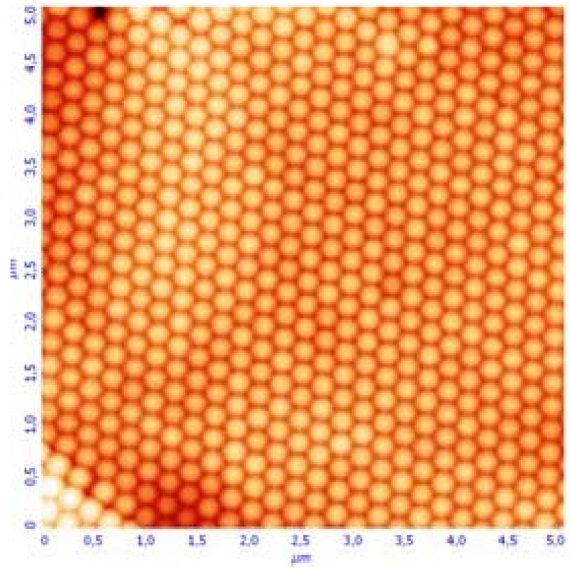

AFM image of the top surface of the opal formed by spin-coating technique of 236 nm diameter polystyrene spheres.

A.Chiappini, C. Armellini, A. Chiasera, M. Ferrari, L. Fortes, M. Clara Gonçalves, R. Guider, Y. Jestin, R Retoux, G. Nunzi Conti, S. Pelli, Rui M. Almeida, and G.C. Righini. "An alternative method to obtain directs opal photonic crystals structures" Journal of Non-Crystalline Solids 355 (2009) pp. 1167-1170

Polystyrene monosized spheres

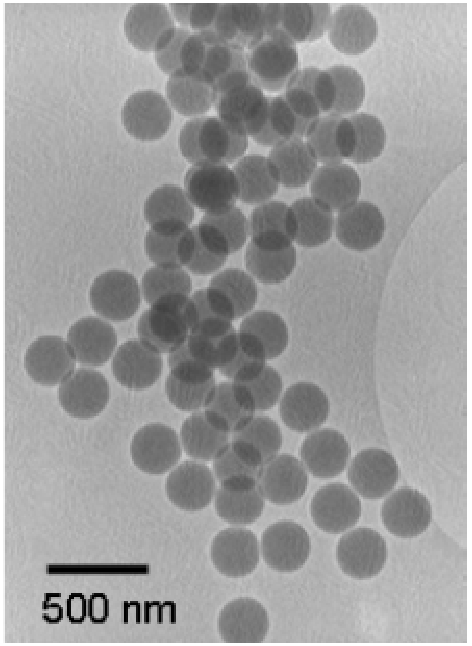

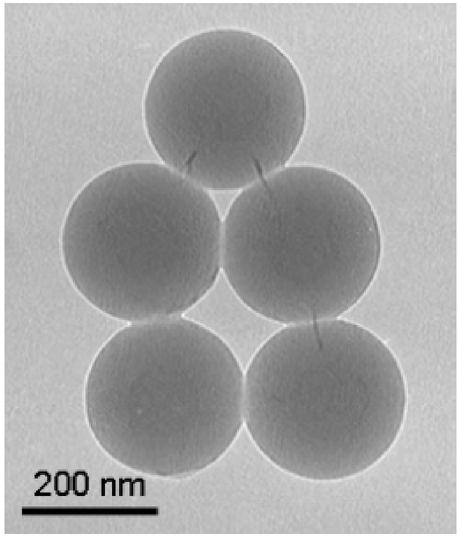

Single-stage polymerization process ***based on formation and growth of*** ***polymeric nuclei dispersed*** ***in an emulsion constituted by water, styrene, potassium persulfate (KPS) and sodium docecyl sulfate (SdS).***

HRTEM characterization of polystyrene spheres synthesized by microemulsion, where an average dimension of 236 nm with a polidispersivity of about 3% is determined

Range 150 ÷ ~ 1000 nm

Control the size of the particles through the concentration of sodium docecyl sulfate.

Self Assembly approach

Self Assembly techniques

Vertical Deposition

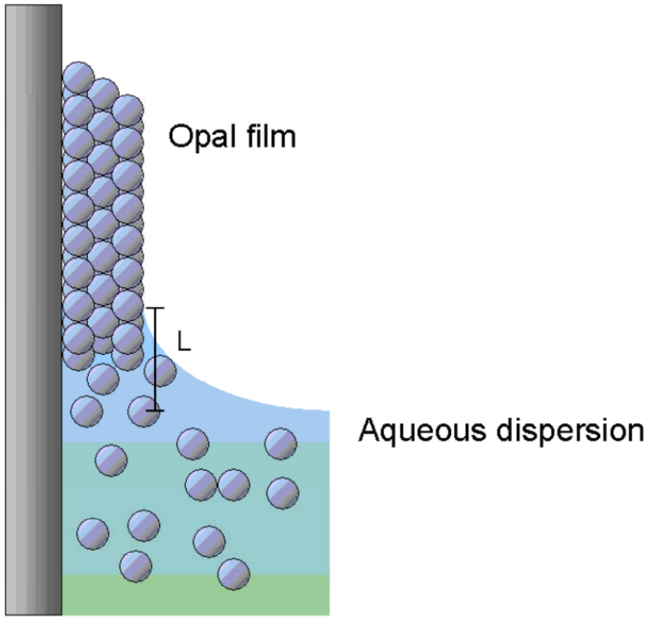

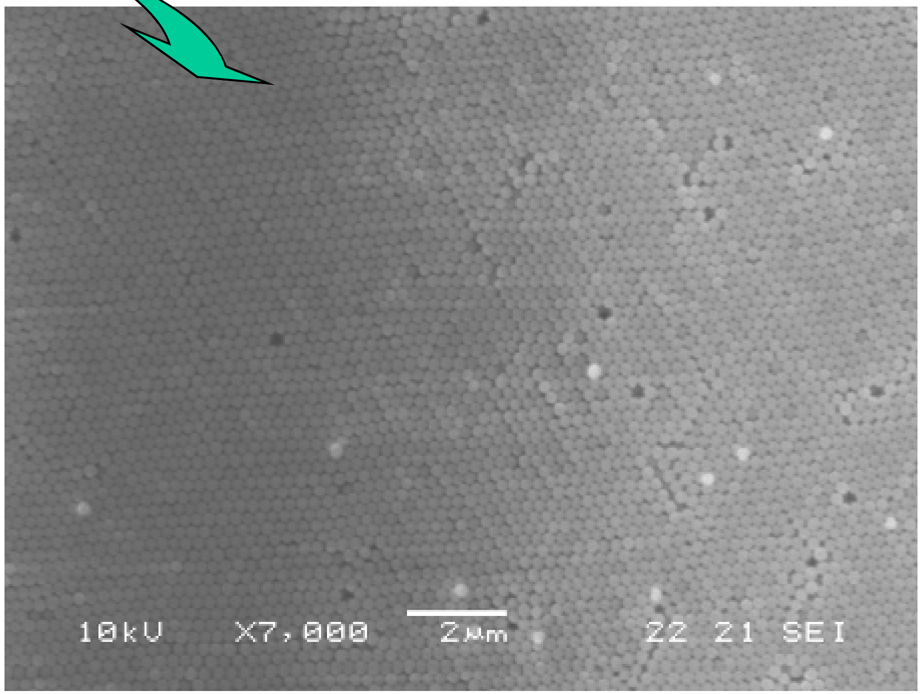

A. Chiappini, C. Armellini, A. Chiasera, M. Ferrari, Y. Jestin, M. Mattarelli, M. Montagna, E. Moser, G. Nunzi Conti, S. Pelli, G.C. Righini, M. Clara Gonçalves, Rui M. Almeida, "Design of photonic structures by sol–gel-derived silica nanospheres" Journal of Non-Crystalline Solids 353 (2007) pp. 674–678.

“Bottom up approch “

Self Assembly techniques

Spin-coating deposition

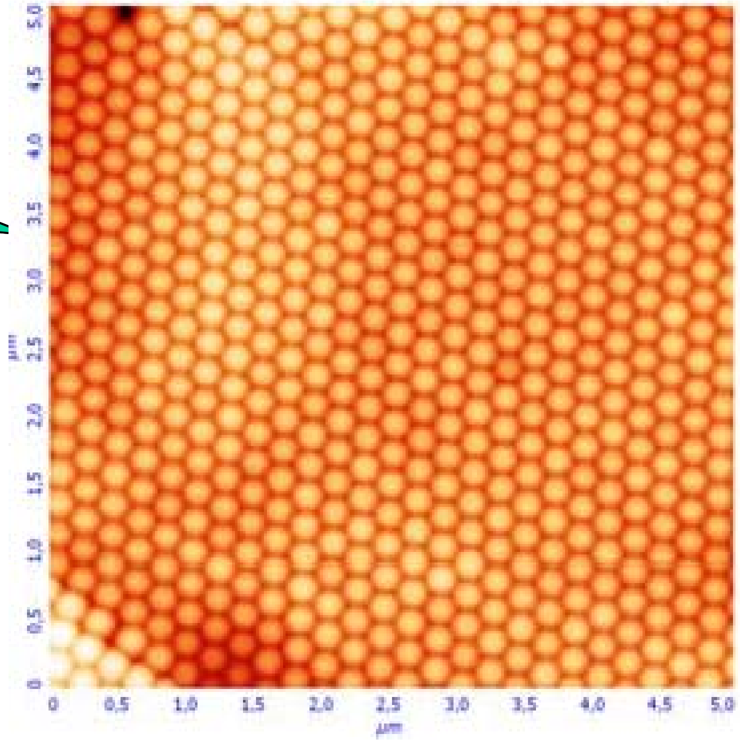

C. Armellini, A. Chiappini, A. Chiasera, M. Ferrari, Y. Jestin, E. Moser, G. Nunzi Conti, S. Pelli, A. Quandt, G.C. Righini, C. Tosello
“Er^{3+} - activated nanocomposite photonic glasses and confined structures”
Optical Materials 31 (2009) pp. 1071-1074.

Silica inverse opals
Latex opals as templates

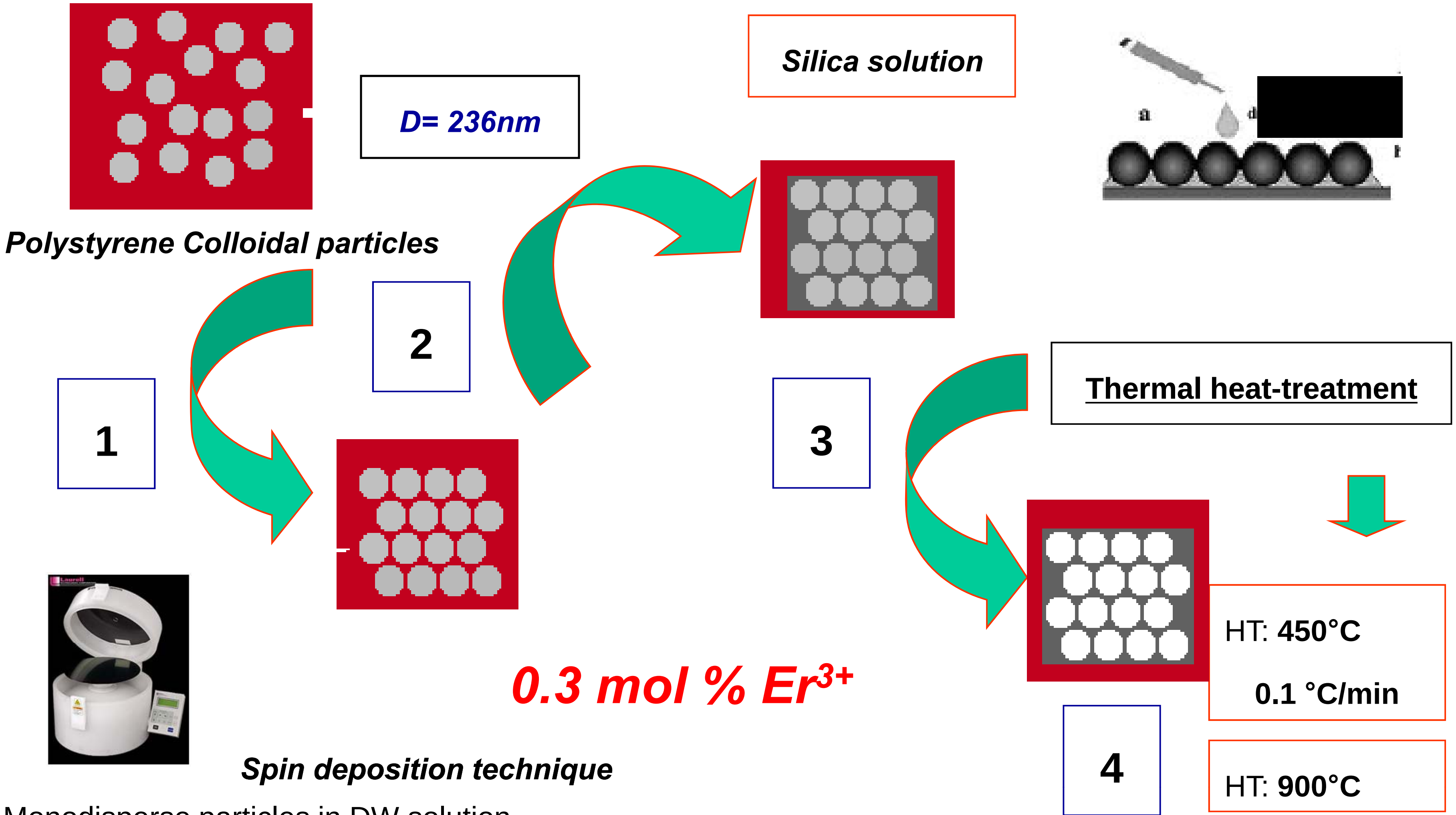

Monodisperse particles in DW solution.

Inverse structure

It's a negative replica of direct opal

(template)

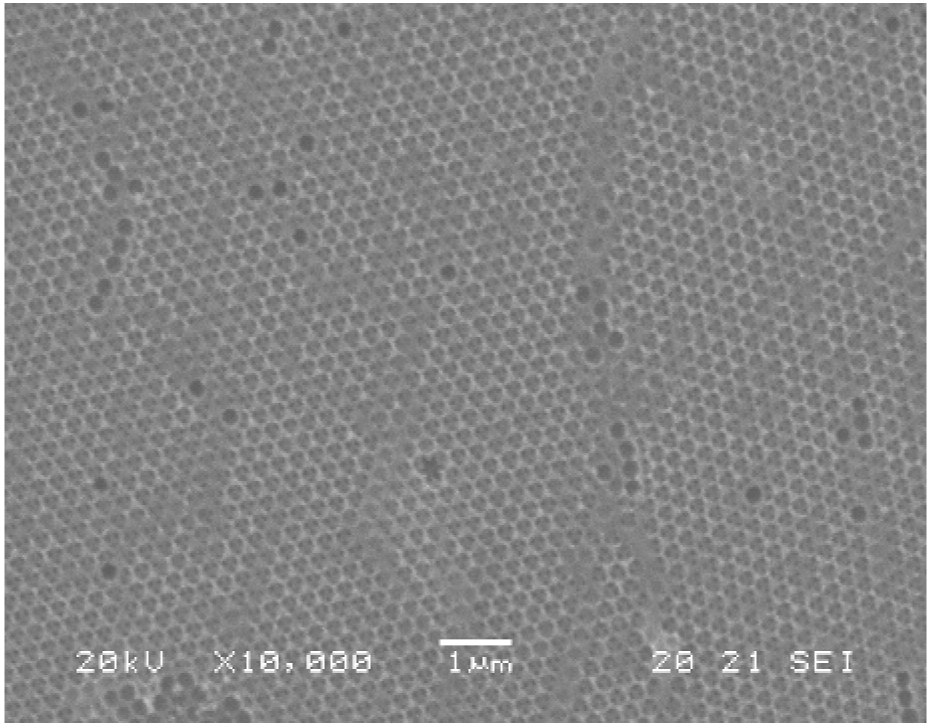

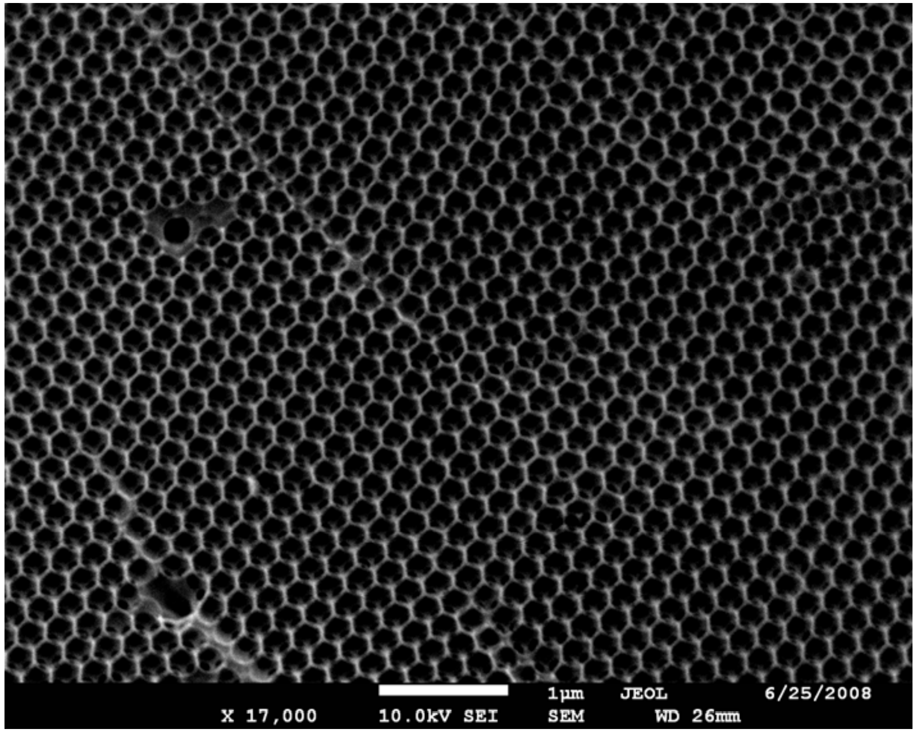

The average dimension of the air-hollows is ~210 nm

Hollow regions of air spheres

well ordered in a triangular lattice

corresponding to the **(111) planes**

of a fcc crystalline strucure.

Optical Properties

Variable incident angle reflectance measurements of inverse opals

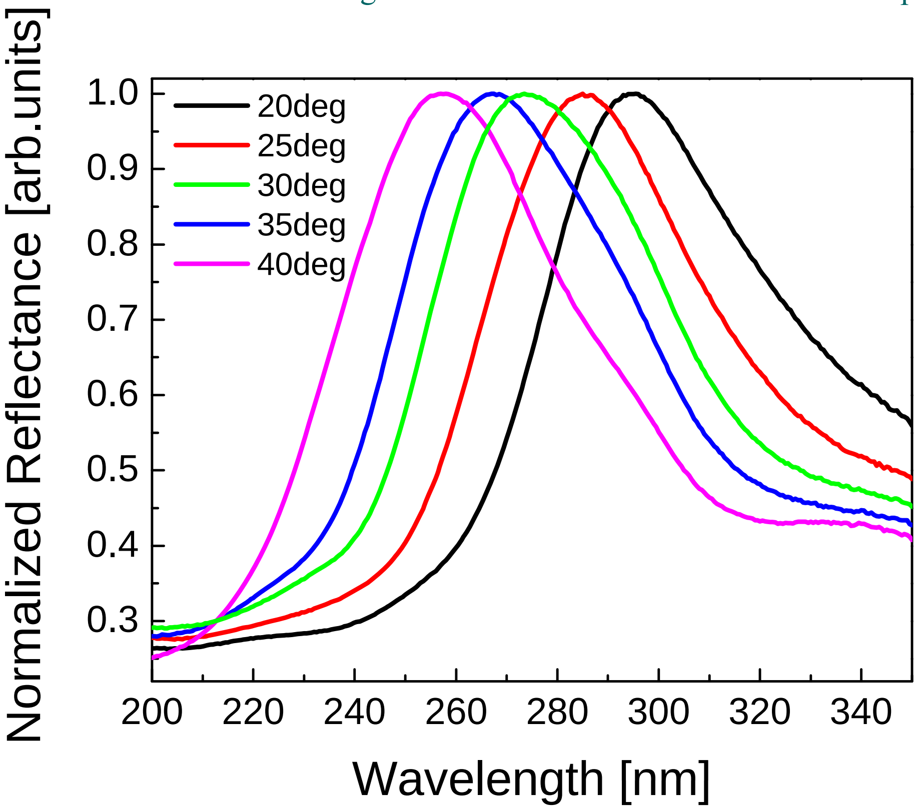

Bragg's Law

$$\lambda = 2 \times 0.816\, D \left(n_{eff}^2 - \sin^2 \theta \right)^{1/2}$$

$$n_{eff}^2 = n_{silica}^2 \cdot f + n_{air}^2 \cdot (1 - f)$$

Filling Factor 23%

Max 26%

Luminescence at 1.5μm

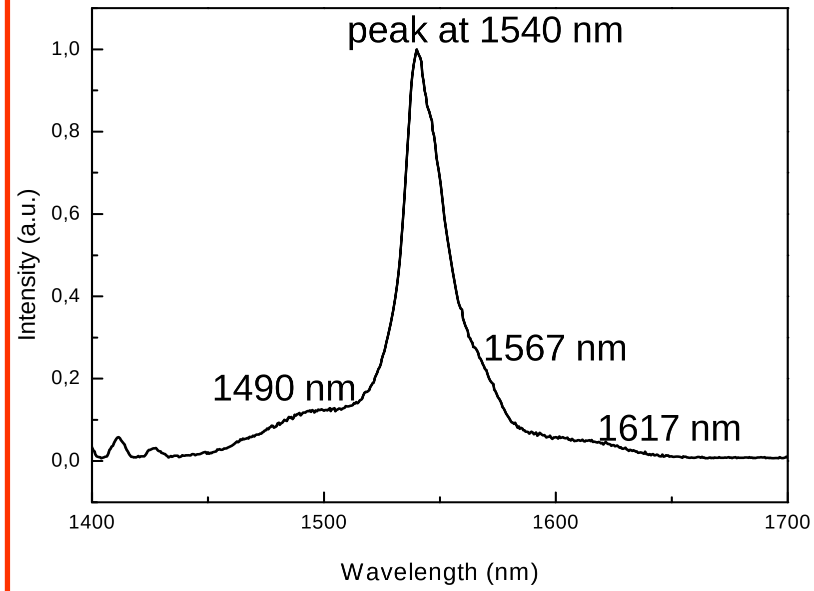

Room temperature photoluminescence spectrum of the $^4I_{13/2} \rightarrow {}^4I_{15/2}$ transition of Er3+ ions

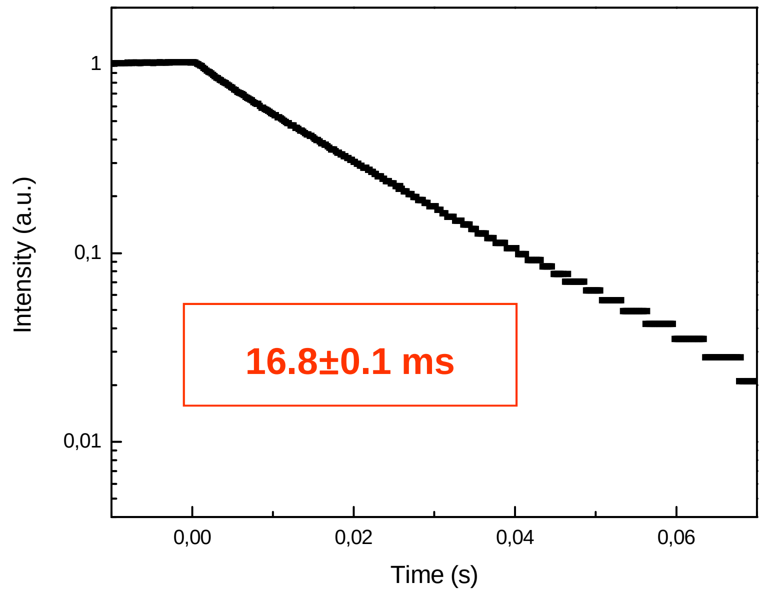

η= 90%

C. Armellini, A. Chiappini, A. Chiasera, M. Ferrari, Y. Jestin, E. Moser, R. Retoux, G. Speranza, L. Minati, G. Nunzi Conti, S. Berneschi, I. Cacciari, S. Pelli, G.C. Righini.
"Fabrication and Characterization of Silica Opals"
Advances in Science and Technology Vol. 55 (2008) pp 118-126.

Photonic Crystals - fundamentals

Why are Photonic Materials special?

Improvement of LED efficiency.

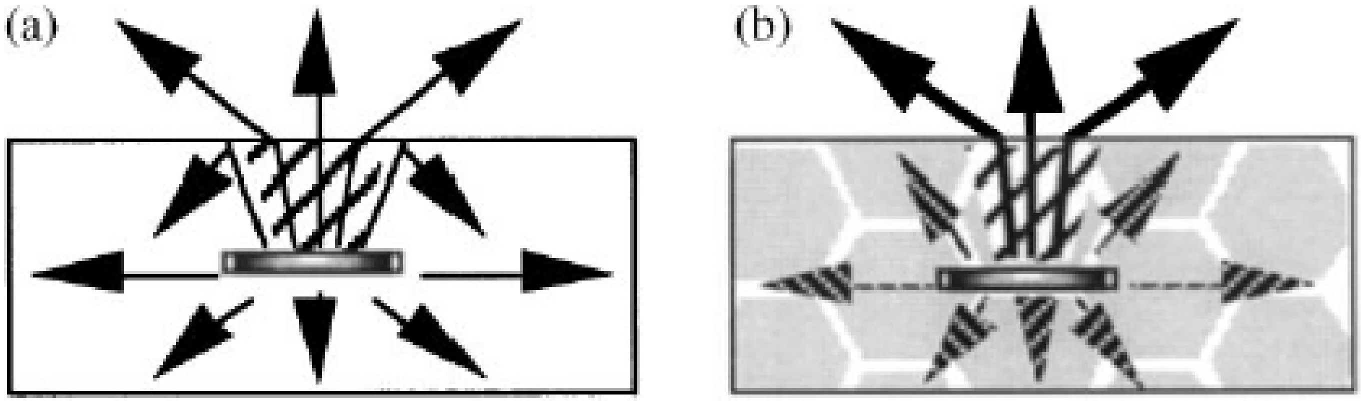

(b) microstructured emitter: light that would not radiate into the emission cone is suppressed by the photonic crystal, i.e. there are no modes for the emission to radiate into, so all spontaneous emission is channeled into the "useful" modes of the device. In principle, the external effiency of such a device can reach the internal efficiency of the material of > 90%.

Photonic Crystals - application

Superprism effect

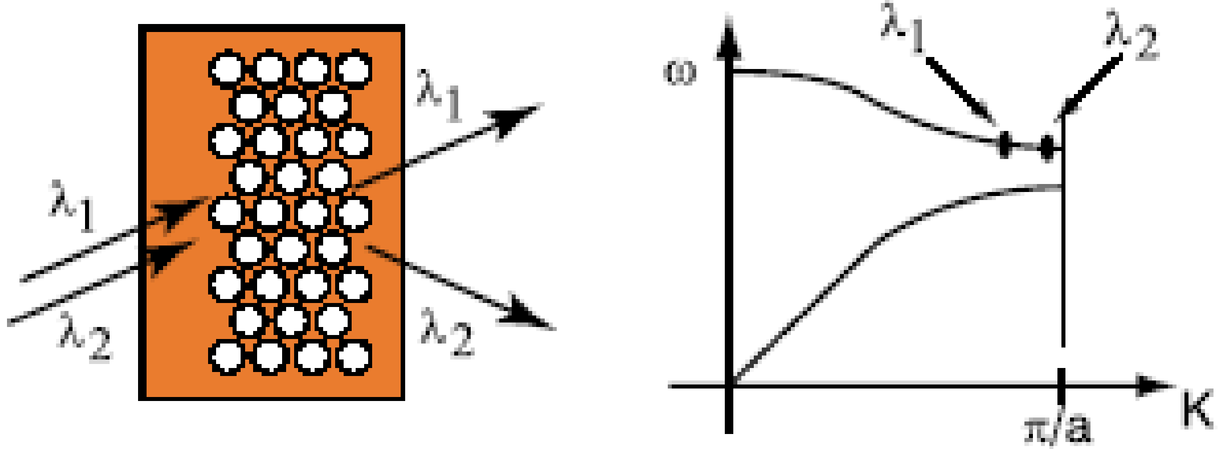

The figure shows how the dispersion properties of a photonic crystal can be used. Due to the high dispersion of wavelengths near the band edge, it is possible to separate the spectral contents of an incoming multi-wavelength signal. This particular effect is known as "superprism"

Photonic Crystals - application

Superprism effect

The self-organized 3D photonic crystal, with the stacking structure analogous to that of simple hexagonal graphite, employed to demonstrate superprism effect in the optical frequency region.

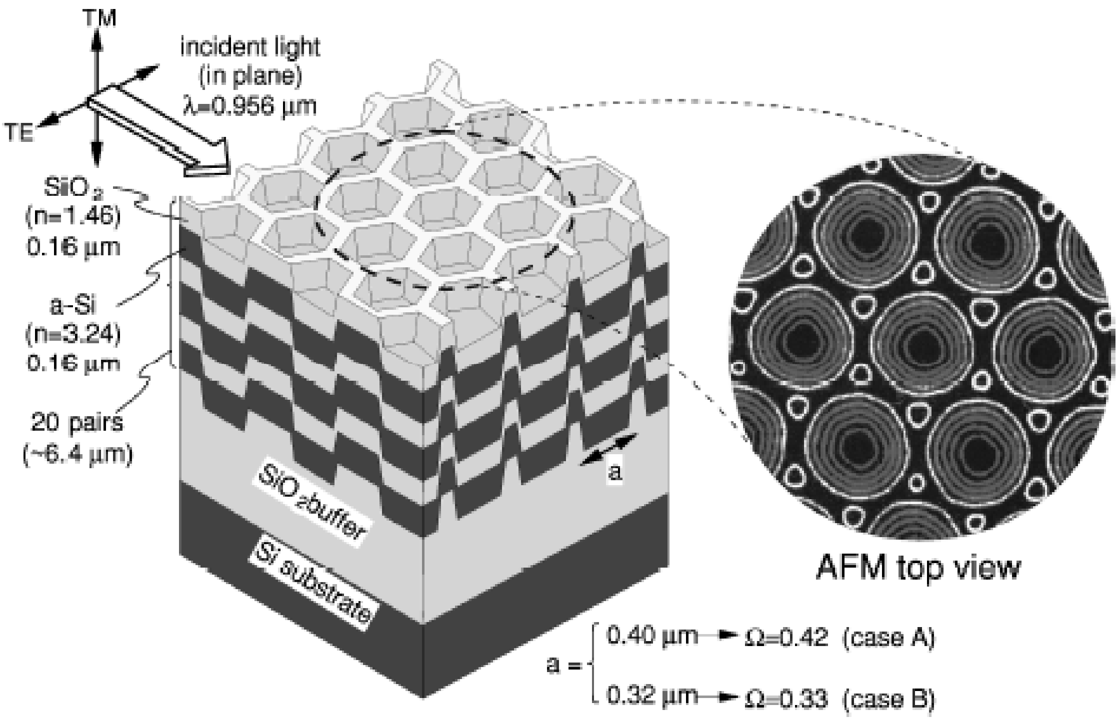

✓H. Kosaka, T. Kawashima, A. Tomita, M. Notomi, T. Tamamura, T. Sato, and S. Kawakami "Superprism phenomena in photonic crystals", Phys. Rev. B 58 (1998) pp. R10 096-R10 099.

Photonic Crystals - application

Superprism effect

Photographs showing light-beam swing inside the photonic crystal. The tilting angle of the incident light was slightly altered from +7° (left) to -7° (right). Both paths show negative bending. The incident light has a wavelength 956 nm (λ/a=0.33) with TM polarization. The crystal size is 0.5 mm x 0.5 mm.

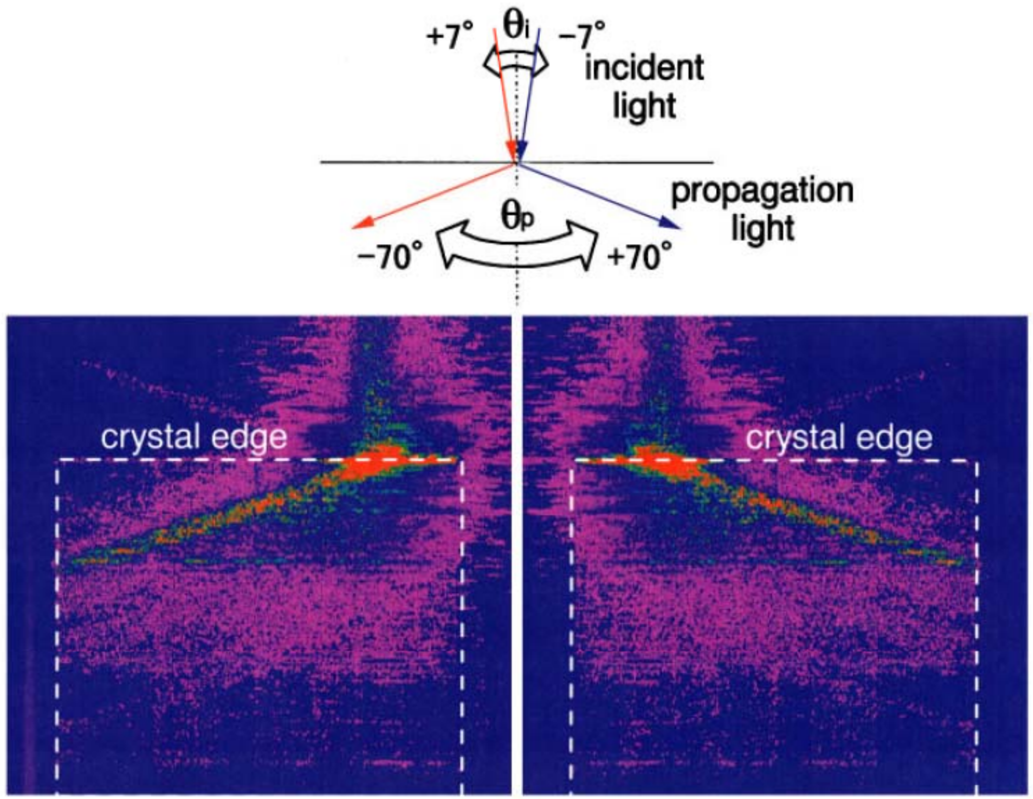

✓H. Kosaka, T. Kawashima, A. Tomita, M. Notomi, T. Tamamura, T. Sato, and S. Kawakami "Superprism phenomena in photonic crystals", Phys. Rev. B 58 (1998) pp. R10 096-R10 099.

Photonic Crystals - application

Superprism effect

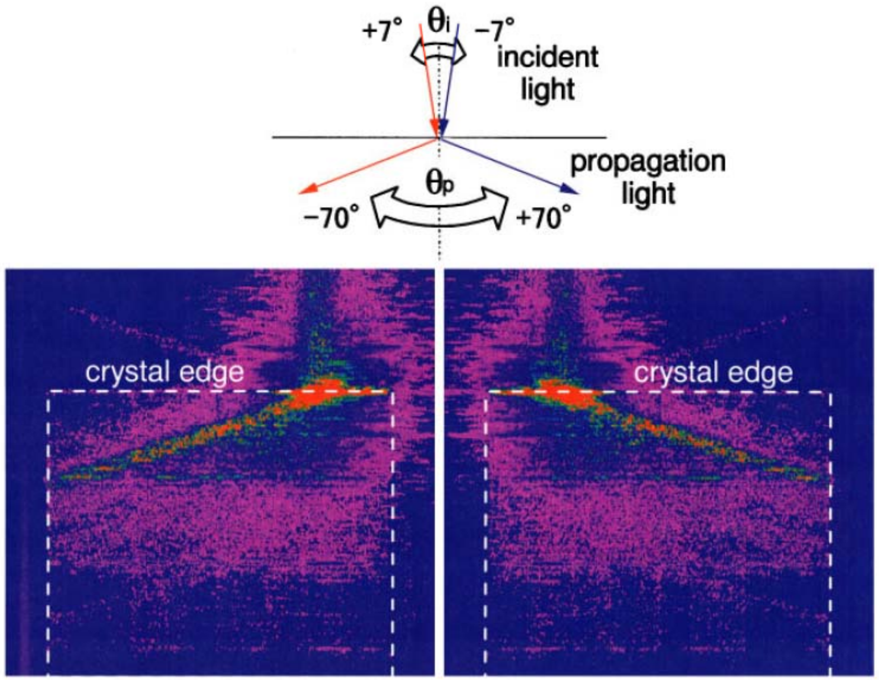

If Snell's law is applied without regard to the photonic band anisotropy, this phenomenon implies a *negative refractive index*.

✓H. Kosaka, T. Kawashima, A. Tomita, M. Notomi, T. Tamamura, T. Sato, and S. Kawakami "Superprism phenomena in photonic crystals", Phys. Rev. B 58 (1998) pp. R10 096-R10 099.

Photonic Crystals - application

Superprism effect

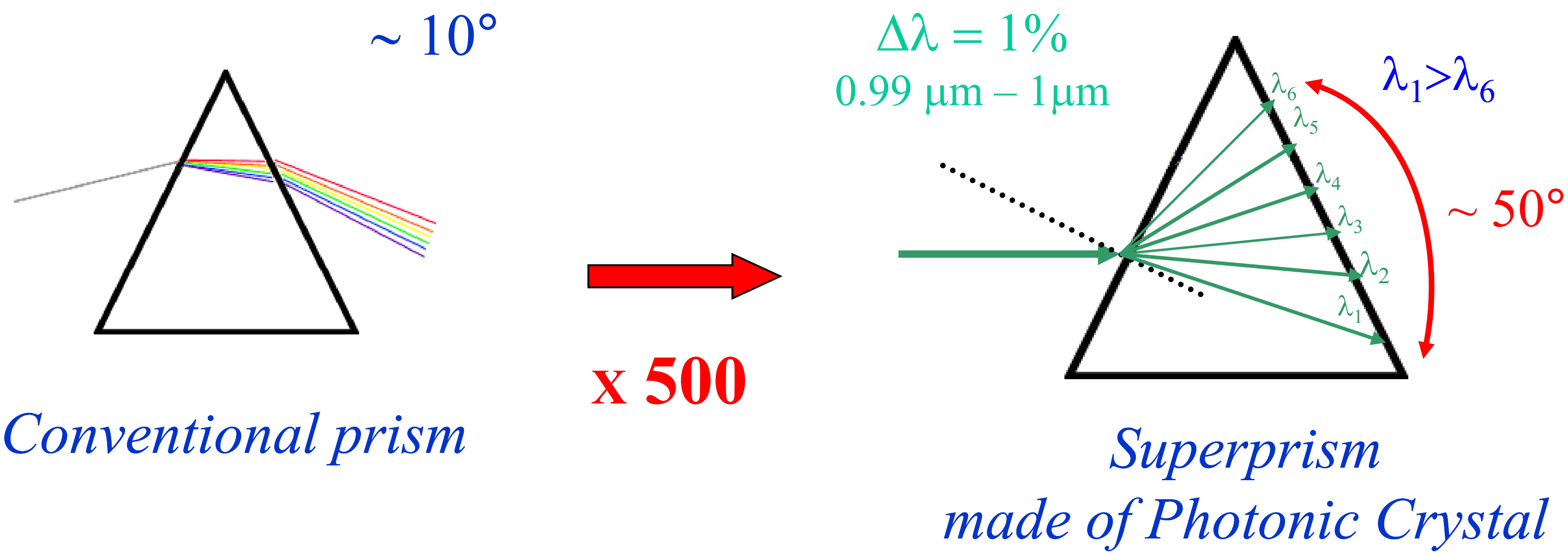

✓H. Kosaka, T. Kawashima, A. Tomita, M. Notomi, T. Tamamura, T. Sato, and S. Kawakami "Superprism phenomenaSuperprism Phenomena in Photonic Crystals: Toward Microscale Lightwave Circuits", Journal of Lightwave Technology, 17 (1999) pp. 2032-2038.

Photonic Crystals - application

Superprism effect

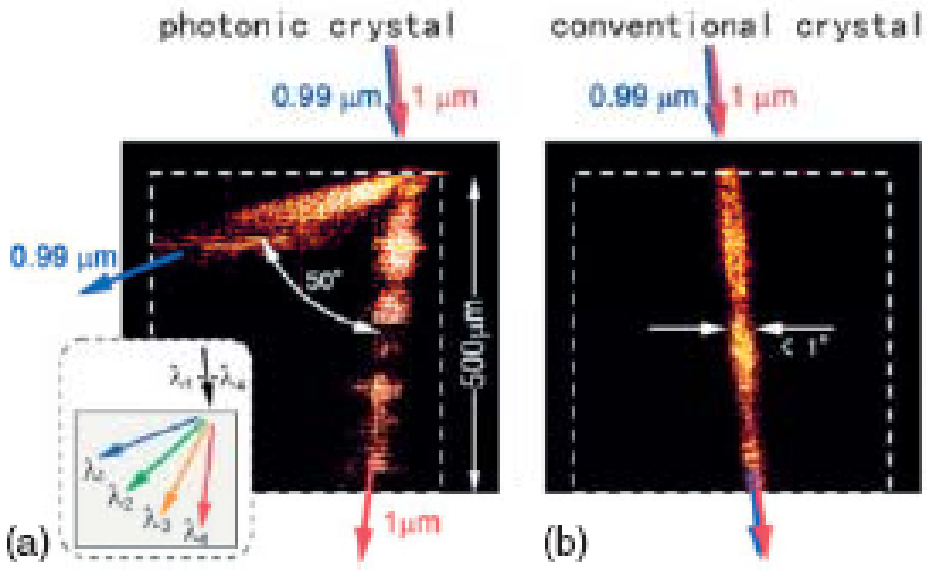

✓H. Kosaka, T. Kawashima, A. Tomita, M. Notomi, T. Tamamura, T. Sato, and S. Kawakami "Superprism phenomenaSuperprism Phenomena in Photonic Crystals: Toward Microscale Lightwave Circuits", Journal of Lightwave Technology, 17 (1999) pp. 2032-2038.

(a) light paths inside a PC with incident light of 0.99-µm and 1.0-µm wavelengths. A large swing reaching 50° was achieved with a slight wavelength change of 1%. The incident light was polarized in the TM mode and tilted at 15° from normal to the crystal edge and

(b) light propagation in a conventional Si crystal under the same condition as (a). The two beams with different wavelengths traced almost the same paths.

Photonic Crystals - application
Superprism effect: 1D superprism (plan view)

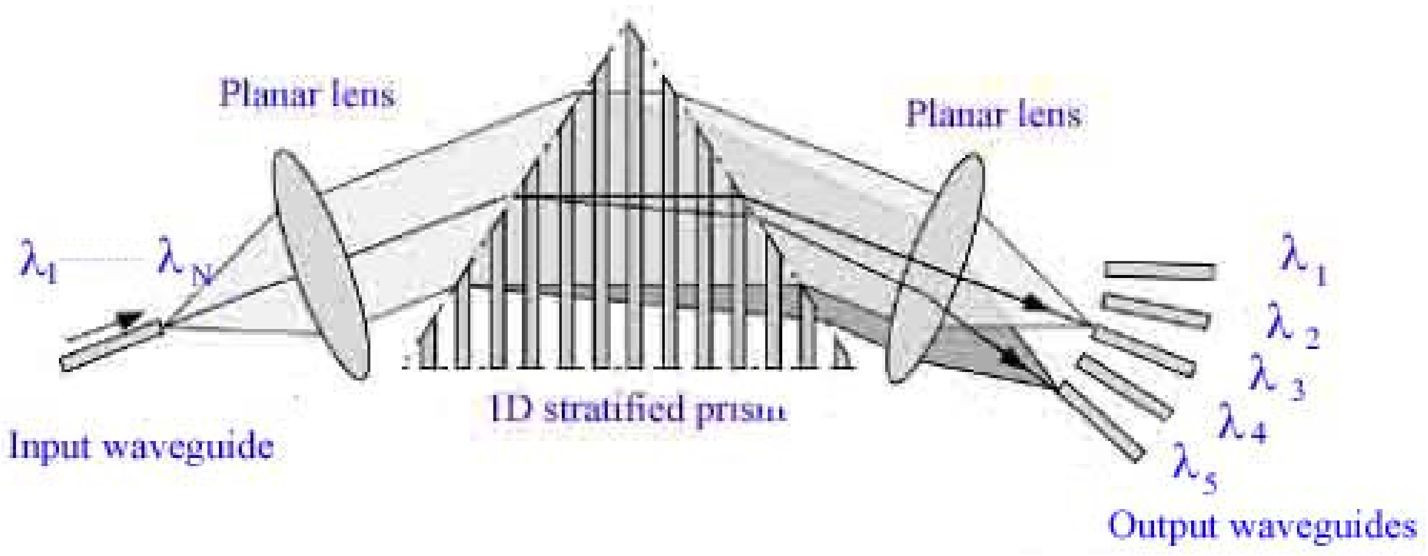

✓A. Bakhtazad, A.G. Kirk, "**Superprism effect with planar 1-D photonic crystal**", Proceedings of the SPIE, Volume 5360, pp. 364-372 (2004)

Strain Sensor

Material: *Changing the structural color*

external stimulus

naked eyes

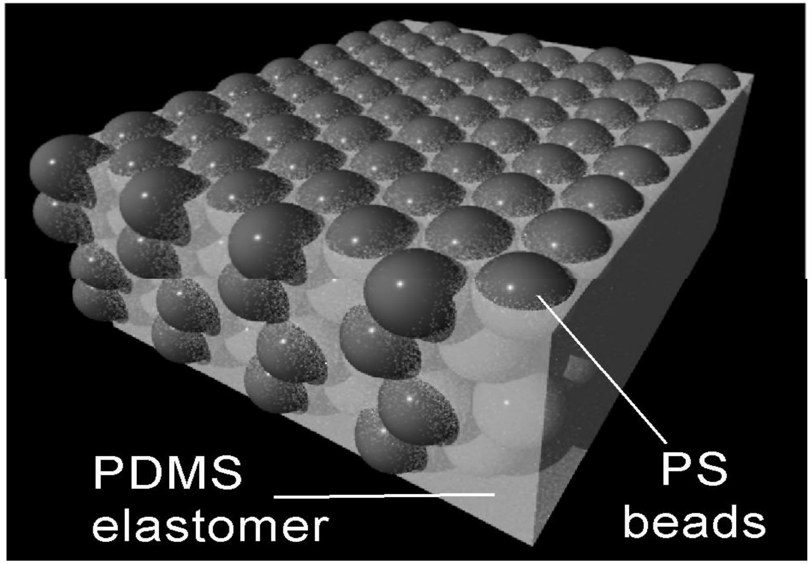

How it works?

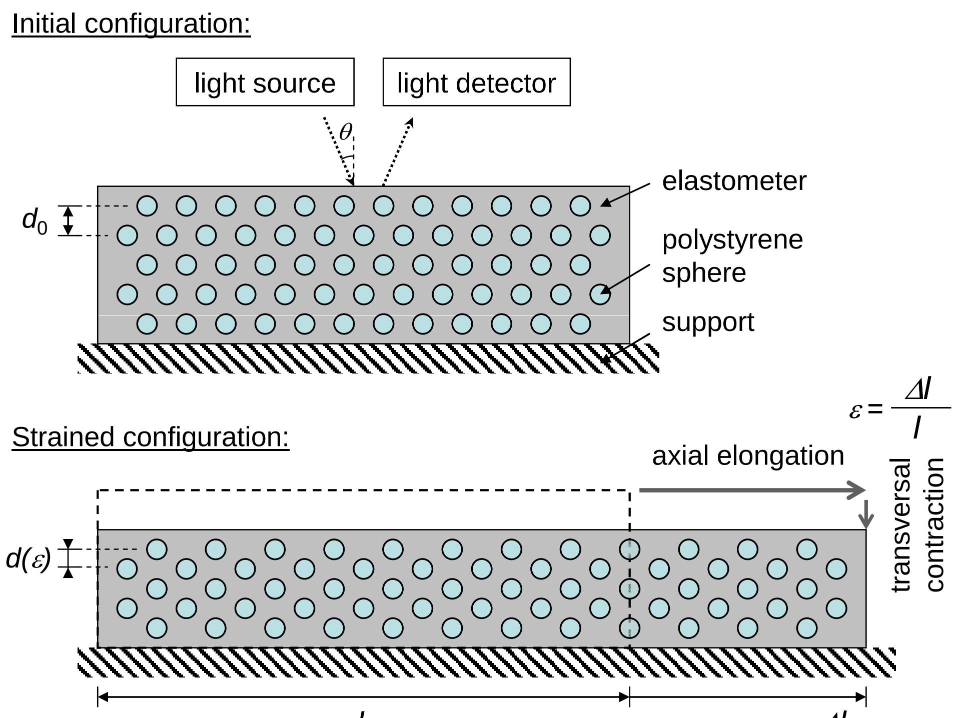

$$\lambda = 2 \cdot d_{111} \cdot n_{eff}$$

Blue shift** of the wavelenght of the diffraction peak as a function of the **applied strain

Strain Sensor

Experimental validation

Initial

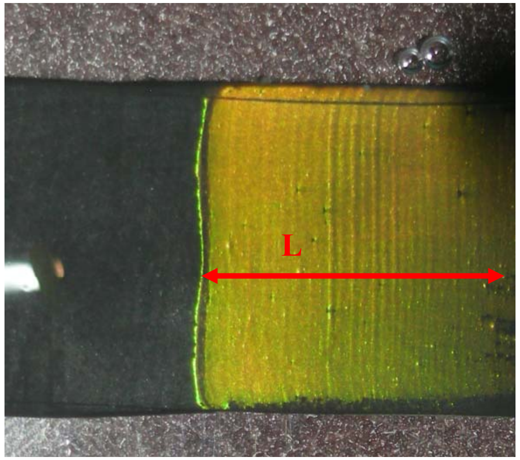

Applied strain

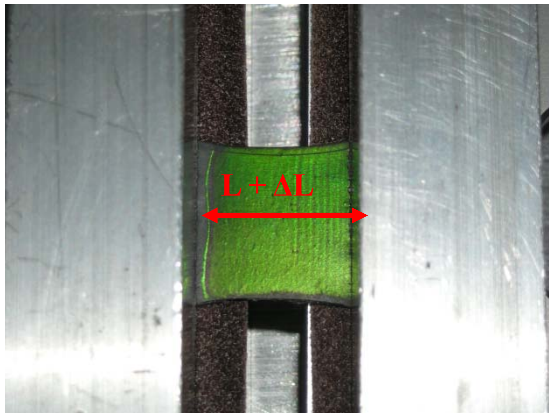

Experimental set-up

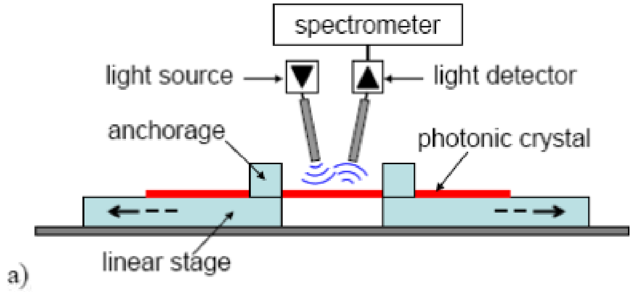

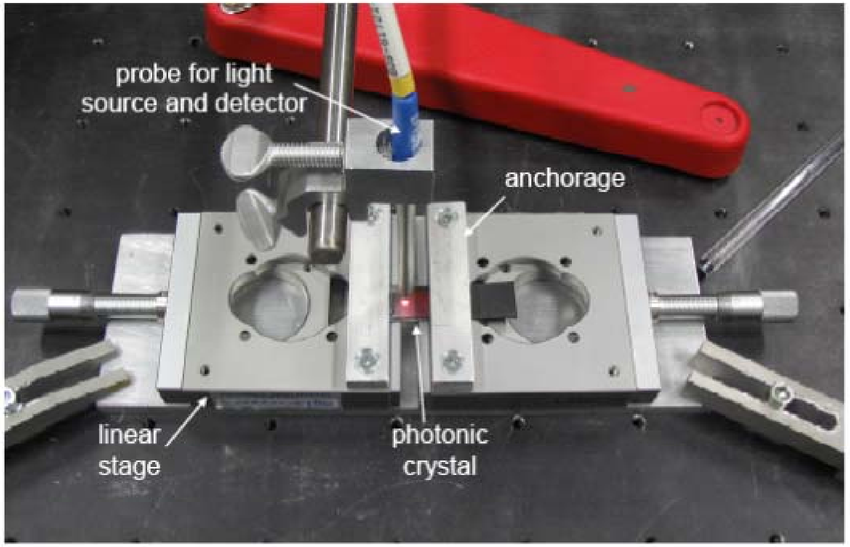

D. Zonta, A. Chiappini, A. Chiasera, M. Ferrari, M. Pozzi, L. Battisti, M. Benedetti, Proc. of SPIE 7292 (2009) pp. 729215-1 - 729215-10.

Strain Sensor

Response Characterisation

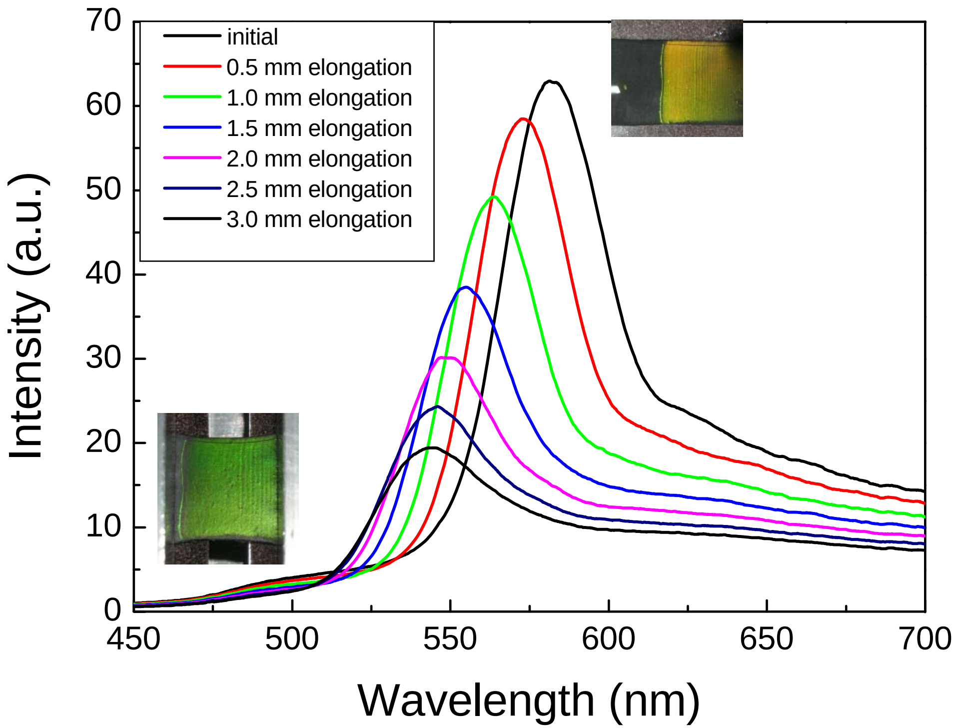

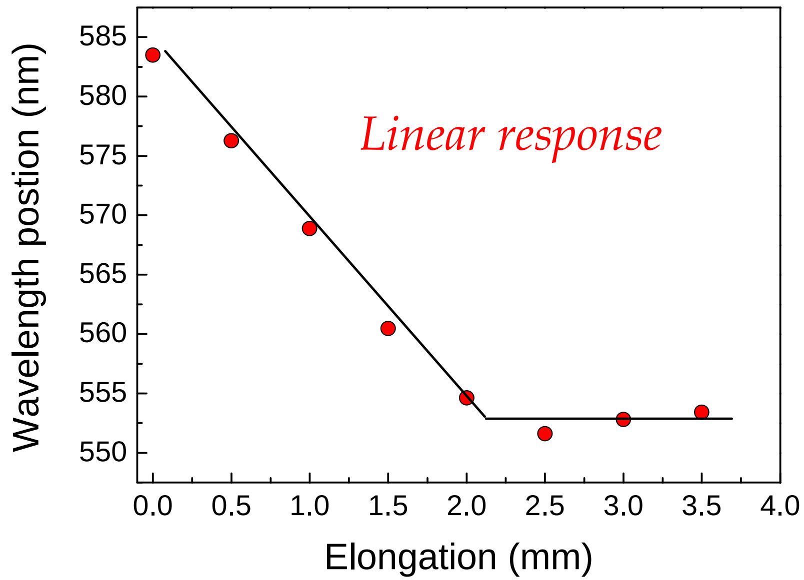

Peak position ***blue shifts*** ***583 to 550 nm***

D. Zonta, A. Chiappini, A. Chiasera, M. Ferrari, M. Pozzi, L. Battisti, M. Benedetti, Proc. of SPIE 7292 (2009) pp. 729215-1 - 729215-10.

Possible applications

– ***SERS substrate***

Metallo – dielectric structures

Gold nanoparticles

How to prepare?

Turkevich Method (1951)

Reduction of Gold ion by citrate ions

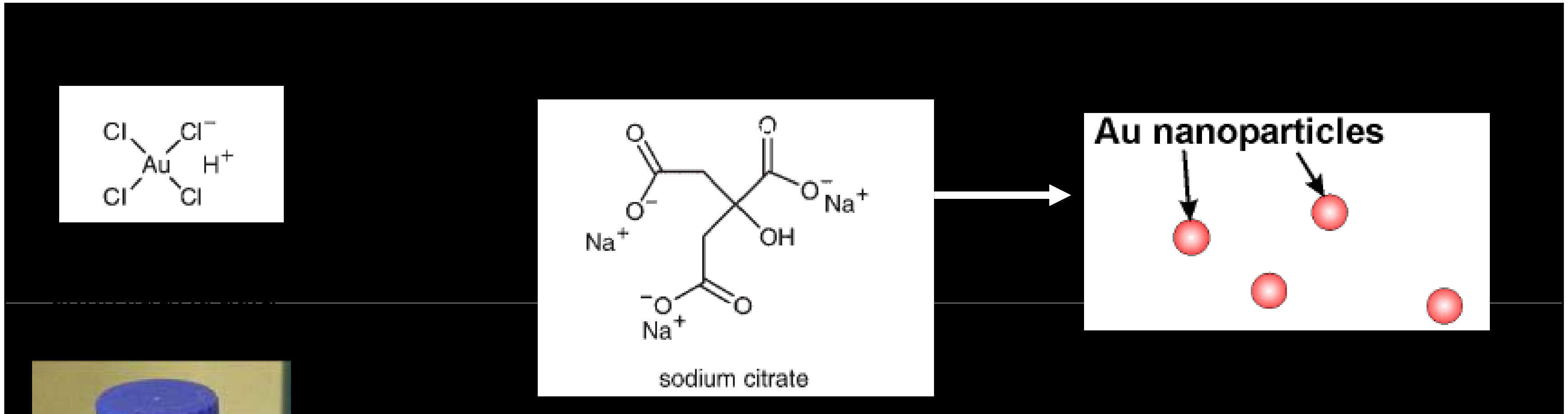

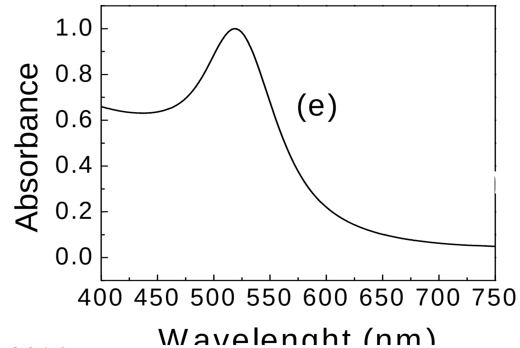

Structural Properties

Inverse ordered structure is still present after immersion process

hollow regions of the air spheres

inner dark holes

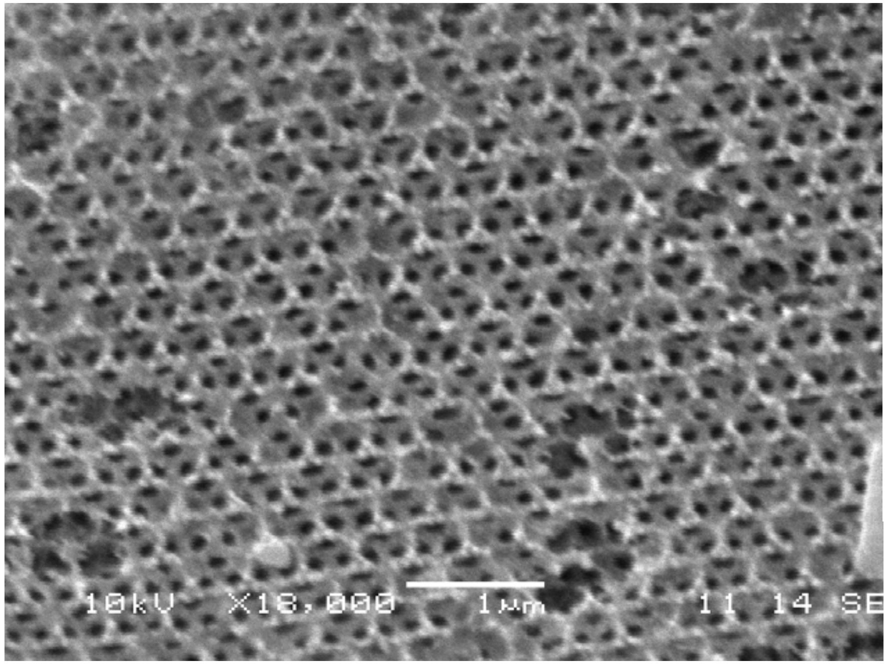

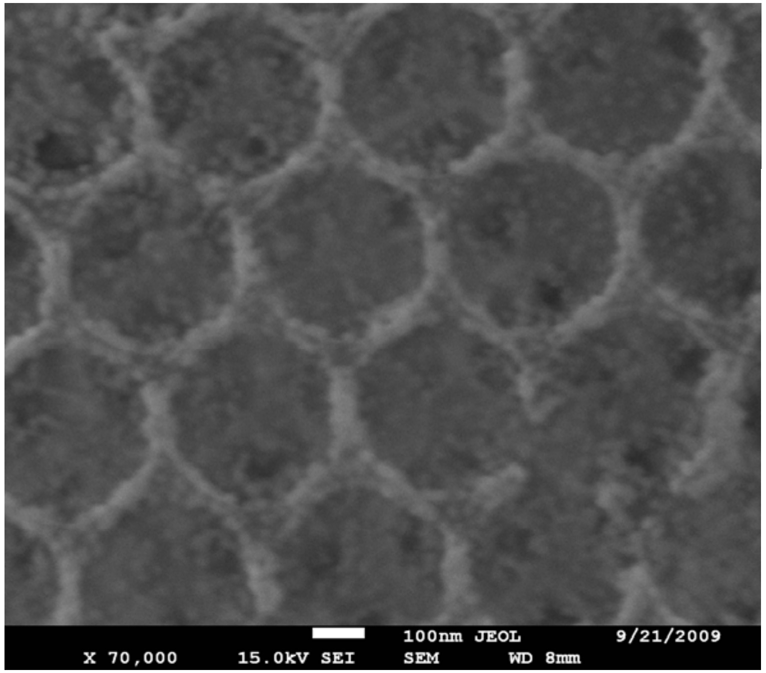

After 2 h immersion time

After 10 h immersion time

Au Nps are attached/immobilized *on the network of the ISO system*

Raman Signal Enhancement

SERS substrate

benzenethiol (BT) as a probe molecule

$1x10^{-3}M$

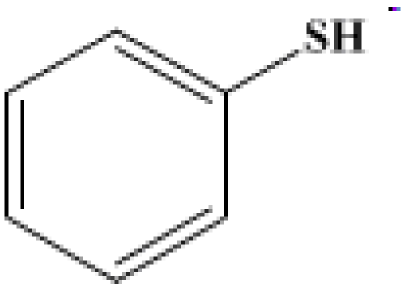

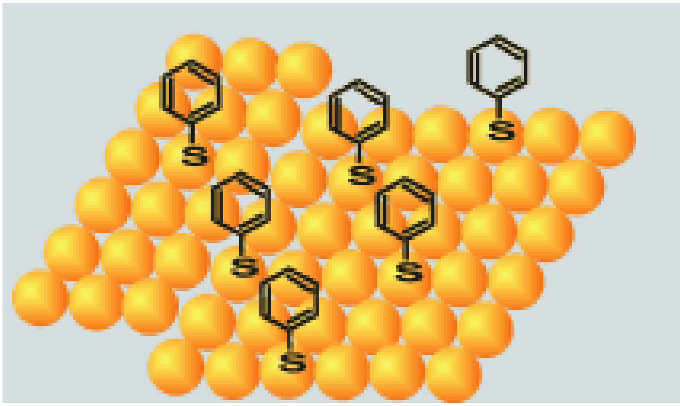

using a 10 s accumulation time, incidence power 100 μW.

to evaluate the efficiency of the MDCS

we have compared the Raman signal obtained for these structures with those collected :

b) on a gold film (GF) deposited by sputtering

c) on ISO spotted with a 5 μl drop of pure BT and left to dry out (ISO_BT).

Raman Signal Enhancement

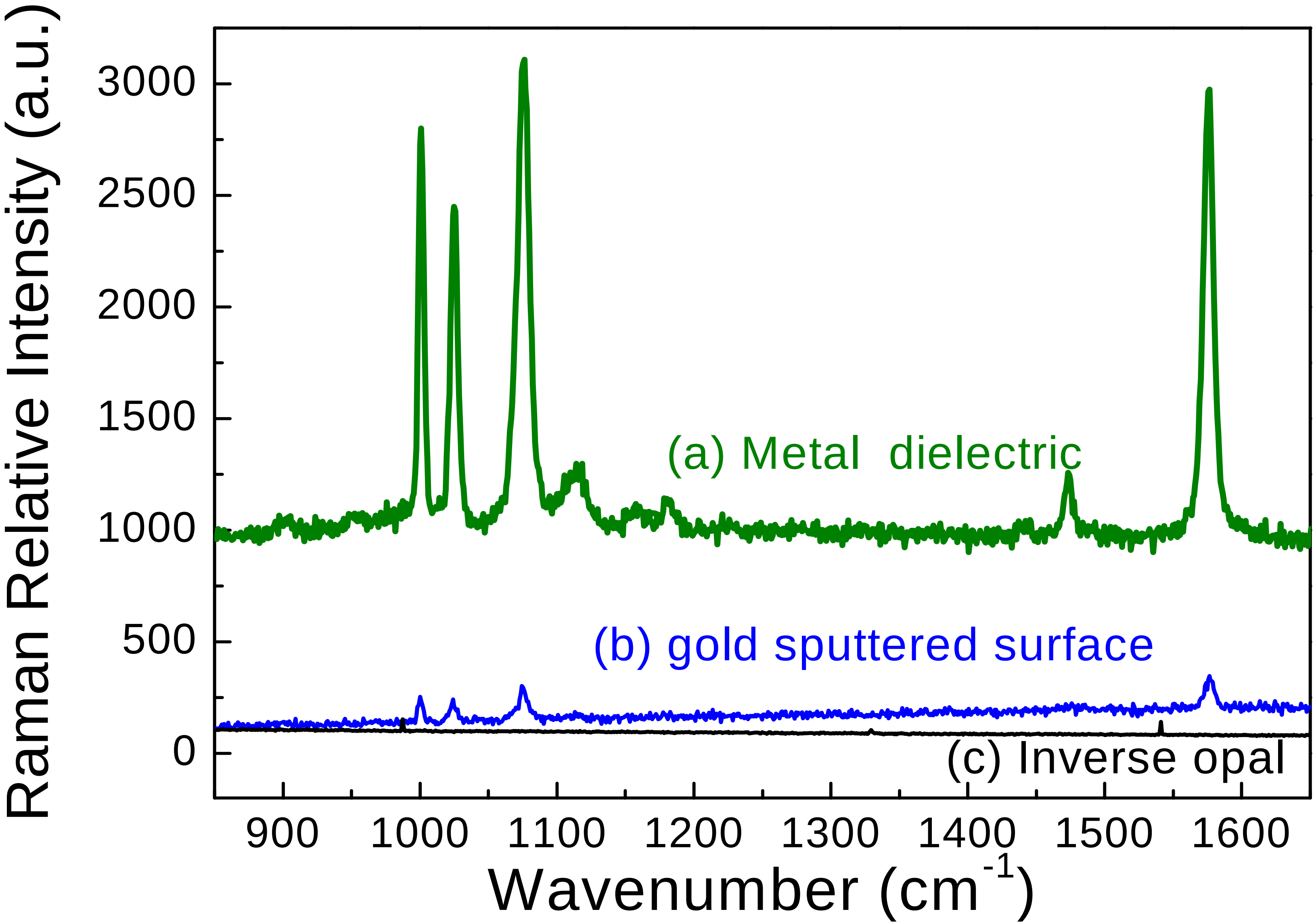

CNR DSFTM
Scienze fisiche e tecnologie della materia
CSMFO Lab. http://www.tn.ifn.cnr.it/
Consiglio Nazionale delle Ricerche
Istituto di Fotonica e Nanotecnologie - Unità di Trento
FONDAZIONE BRUNO KESSLER

PHOTONIC CRYSTALS

HIGH QUALITY FACTOR 1-D Er^{3+}-ACTIVATED DIELECTRIC MICROCAVITY FABRICATED BY RF-SPUTTERING

Dipartimento di Fisica Scuola di Dottorato Università di Perugia 09 aprile 2014

Fabrication Protocol – Target composition

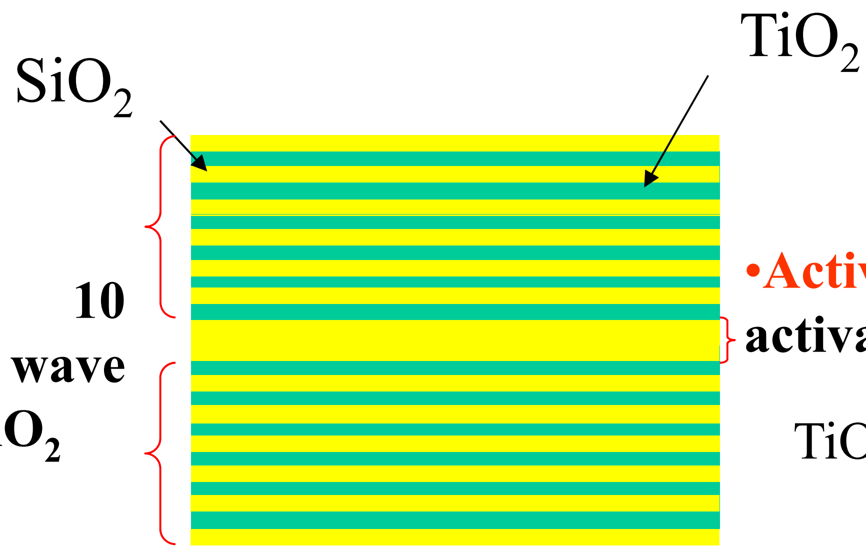

- **Bragg Mirror 10 alternated quarter wave layers TiO_2 and SiO_2**

- **Active layer half wave SiO_2 activated with Er^{3+} ions.**

TiO_2 n = 2.20 (@ 1550 nm)

SiO_2 n = 1.44 (@ 1550 nm)

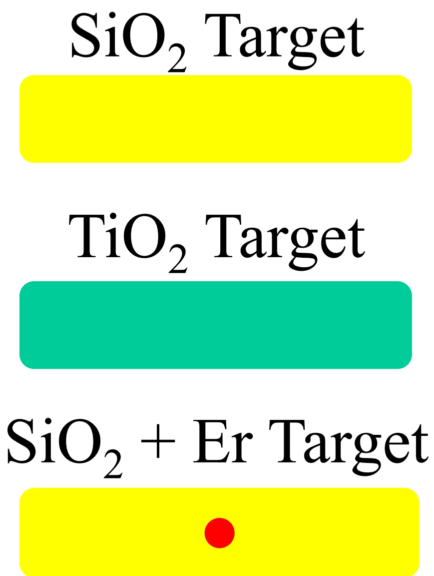

Substrate: v-SiO_2, dim. 7 x 3cm

Deposition is performed by sputtering alternatively the targets of silica and titania. The depositions were tailored to reach the appropriate thicknesses to obtain a cavity resonance centred at 1.7 μm

Development and optical and spectroscopic diagnostic of photonic materials and structures

1-D microcavities fabricated by RF-sputtering

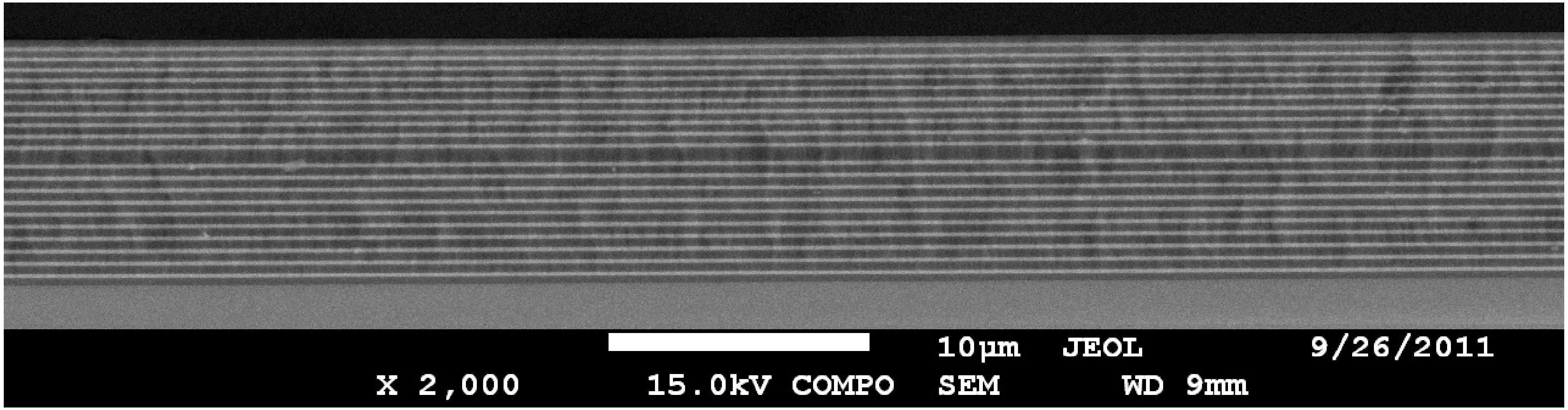

Bragg Mirror: 20 alternated quarter wave layers TiO_2 (170 nm) and SiO_2 (320 nm).
Active layer: half wave (640 nm) SiO_2 activated with 0.2 mol % of Er^{3+}.
The dark regions corresponds to SiO_2 and the white regions corresponds to TiO_2

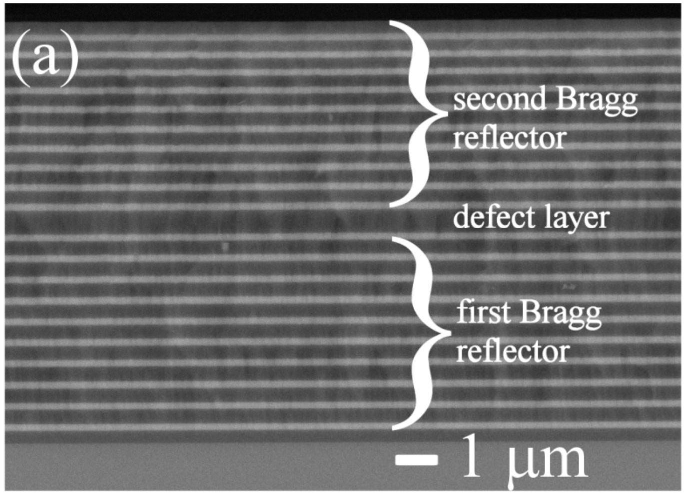

S. Valligatla, A. Chiasera, S. Varas, N. Bazzanella, D.N. Rao, G.C. Righini, M. Ferrari, "High quality factor 1-D Er^{3+}-activated dielectric microcavity fabricated by RF-sputtering", Optics Express, Vol. 20 Issue 19, pp.21214-21222 (2012)

Transmission measurements

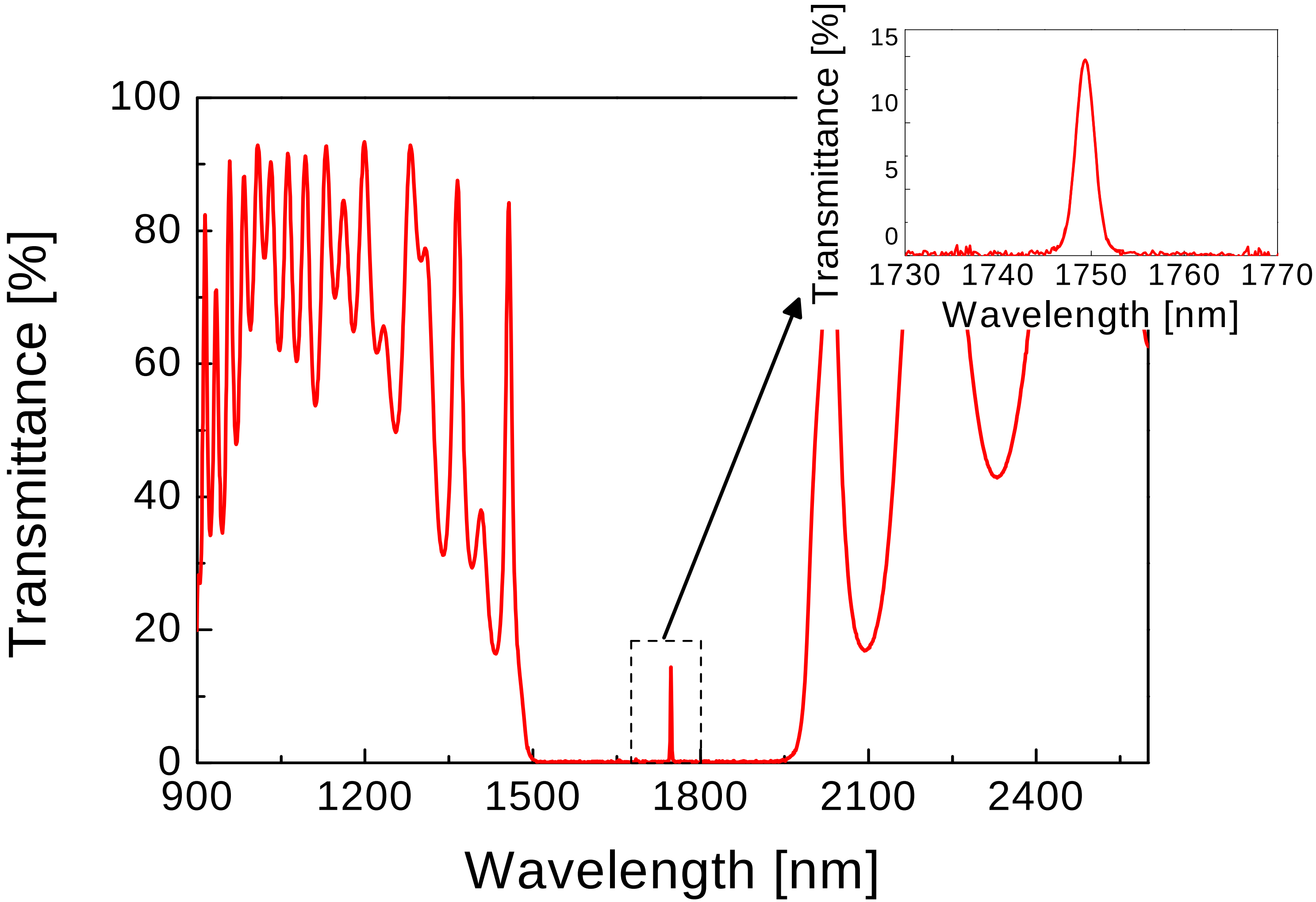

Transmittance spectrum of the cavity with two Bragg reflectors. The stop band range from 1490 to 1980 nm. The cavity resonance corresponds to the sharp maximum centred at 1.749 µm. The FWHM of the resonance is 1.97 nm that correspond to a quality Q factor of 890.

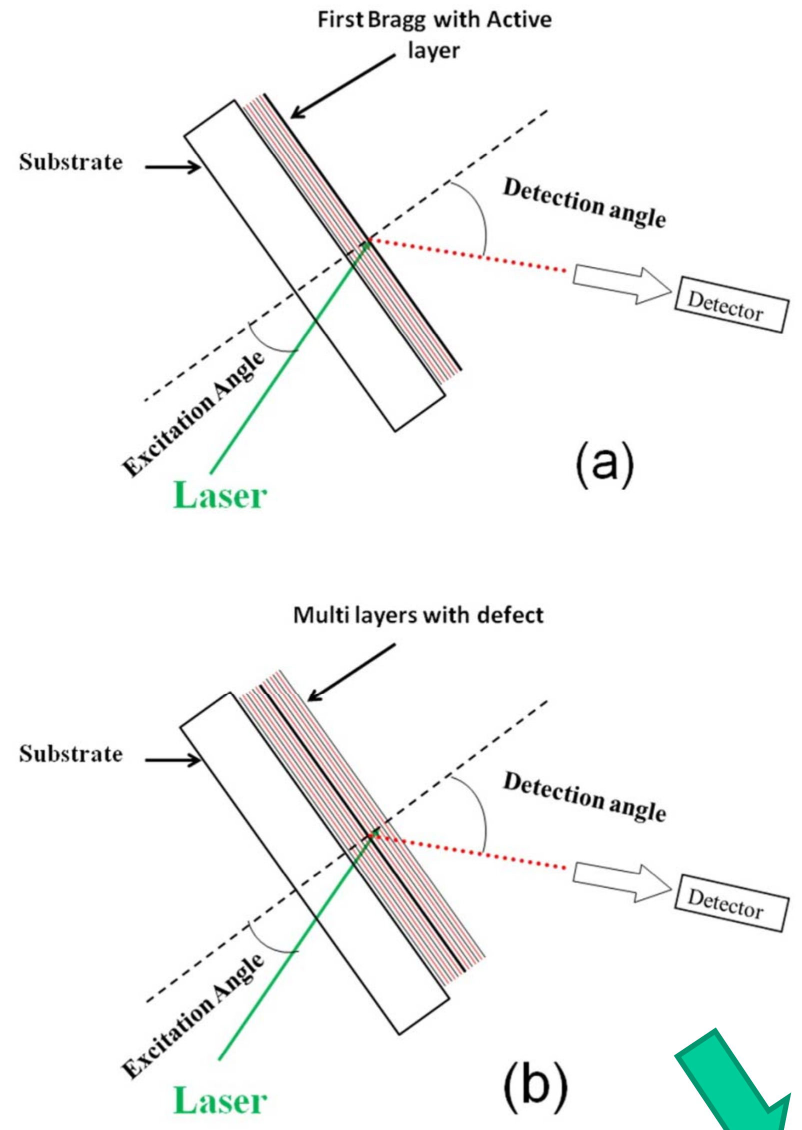

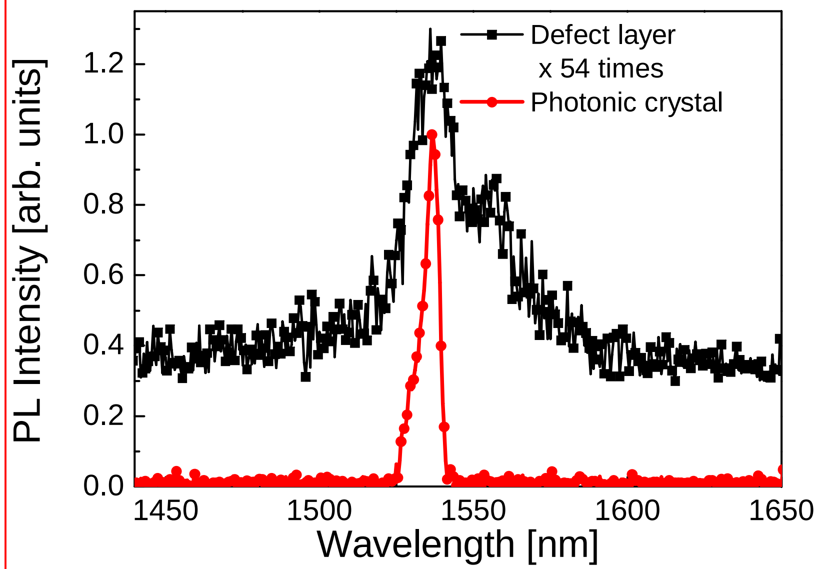

$^4I_{13/2} \rightarrow ^4I_{15/2}$ photoluminescence spectra of the cavity activated by Er^{3+} ion in 1-D photonic crystal and of the single Er^{3+}-doped SiO_2 active layer with first Bragg mirror. The light is recorded at 50° from the normal on the samples upon excitation at 514.5 nm.

Schematics of the excitation and detection geometries employed for a reliable assessment of the influence of the cavity on the 1.5 mm emission band of Er^{3+} ion.

Fig. (a): configuration employed for the Er^{3+}-activated reference sample:

Fig. (b): configuration employed for the Er^{3+}-activated 1-D microcavity.

CNR DSFTM
Scienze fisiche e tecnologie della materia
CSMFO Lab. http://www.tn.ifn.cnr.it/
Consiglio Nazionale delle Ricerche
Istituto di Fotonica e Nanotecnologie - Unità di Trento
ifn
FONDAZIONE BRUNO KESSLER

SPHERICAL MICRORESONATORS

WHISPERING GALLERY MODES LASER

Dipartimento di Fisica Scuola di Dottorato Università di Perugia 09 aprile 2014

Spherical microresonators WGMs

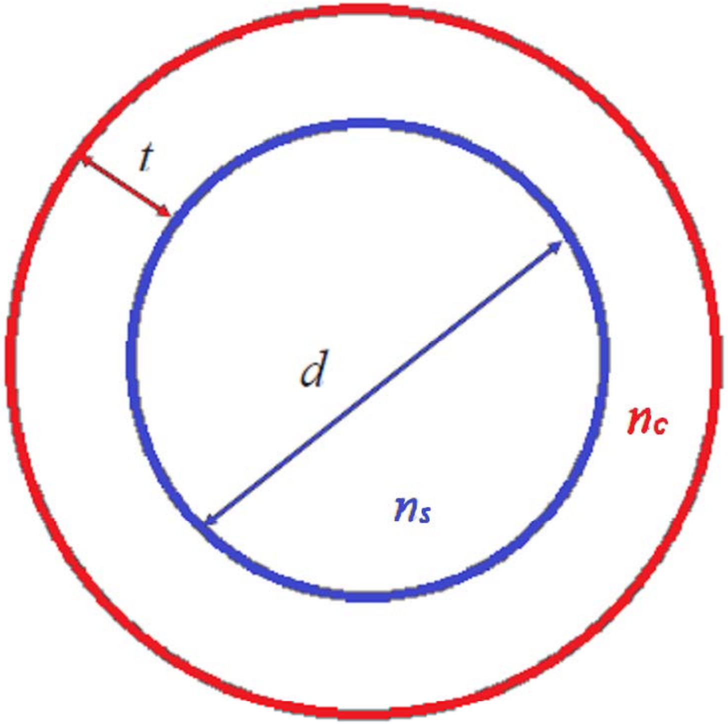

Microsphere of diameter d and refractive index n_s coated by a film of thickness t and refractive index n_c.

G.C. Righini, Y. Dumeige, P. Féron, M. Ferrari, G. Nunzi Conti, D. Ristic, S. Soria., "Whispering gallery mode microresonators: fundamentals and applications", Rivista del Nuovo Cimento 34 (2011) pp. 435-488.

D. Ristić, A. Rasoloniaina, A, Chiappini, P. Féron, S. Pelli, G. Nunzi Conti, M. Ivanda, G.C. Righini, G. Cibiel, and M. Ferrari "About the role of phase matching between a coated microsphere and a tapered fiber: experimental study" Optics Express, 21 (2013) pp 20954-20963

Glass coated microspheres

Silica microspheres fabricated by melting a SMF-28 rod. This glass presents a very low concentration of impurities (<0.3 ppm) and OH groups (<0.2 ppm), the attenuation coefficient is very low (≅ 0.2 dB/km at 1550 nm) The diameters and ellipticity are also reported

	F1	F2	F3	F4	F5	F6	F7	F8	F9
d/μm [±5 μm]	155	135	140	140	140	145	130	155	145
Ellipticity [±1%]	4%	7%	4%	5%	7%	5%	4%	3%	3%

Microscope images of the F5 microsphere before and after coating

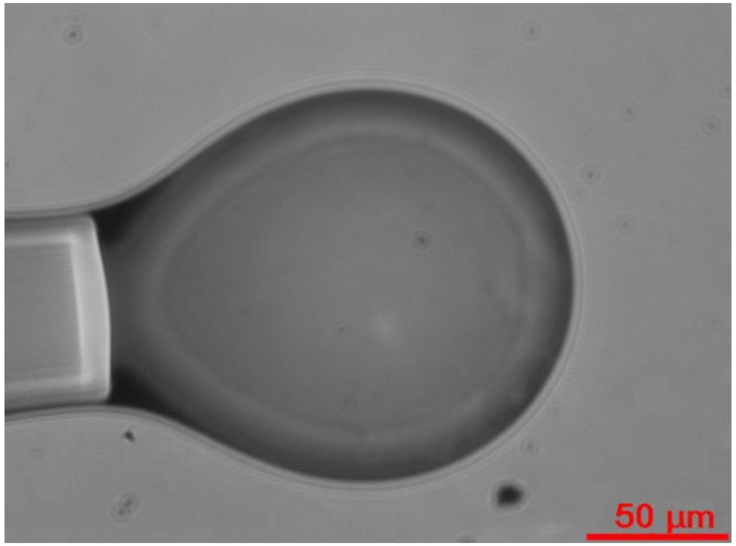

Before coating

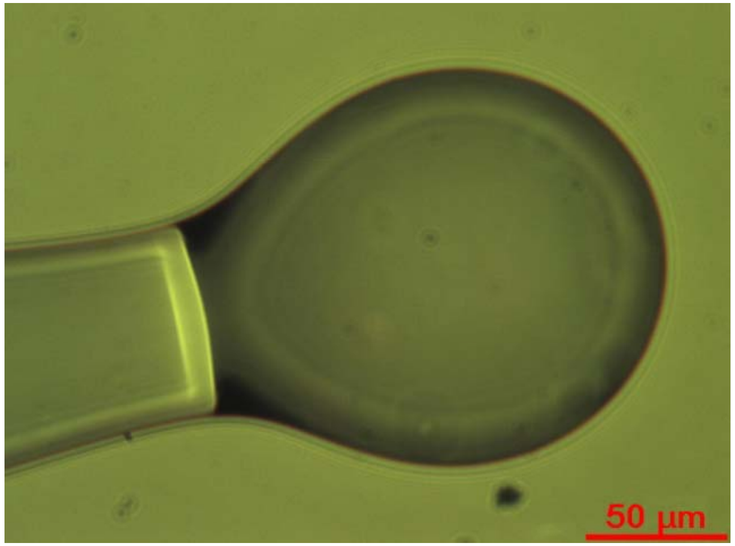

After coating

Glass coated microspheres

A waveguide was prepared as reference using the same sol and the same dip coating technique as for the microsphere in order to estimate the thickness and the refractive index of the coating

Wavelength [nm]	Mode polarization	number of modes	refractive index	thickness [μm]
632.8	TE	3	1.6165±0.0003	1.25±0.01
543.5	TE	3	1.6215±0.0003	1.25±0.01

Thickness, refractive index, and modal parameters of the planar waveguide used as reference for the sol gel coating of the microsphere. Values are obtained by m-line measurement. The film composition was $70SiO_2$-$30HfO_2$ activated with 0.3 mol% Er^{3+}.

Glass coated microspheres

Room temperature photoluminescence spectra and decay curves of the $^4I_{13/2} \rightarrow {}^4I_{15/2}$ transition of Er^{3+} ions for the sol gel coated spherical microresonators and the planar waveguide used as reference. The film composition was $70SiO_2$-$30HfO_2$ activated with 0.3 mo% Er^{3+}.

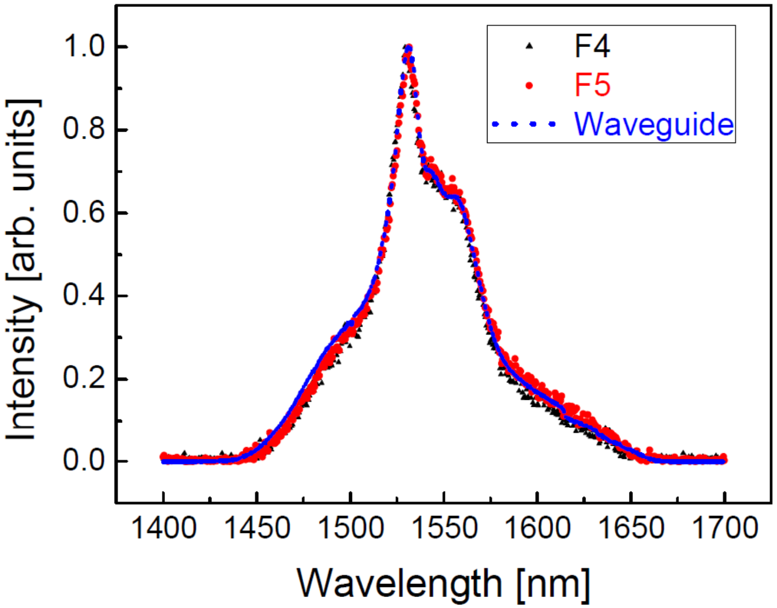

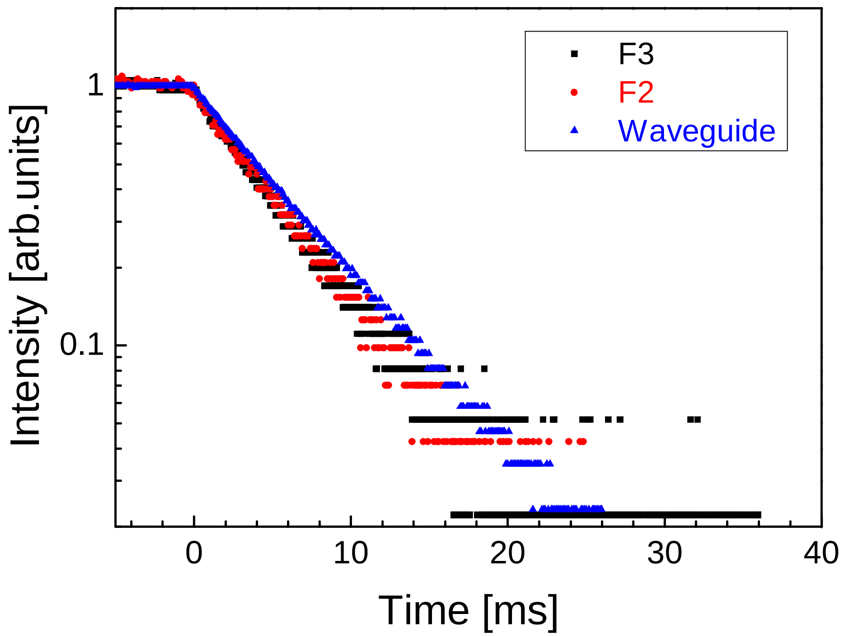

All the photoluminescence spectra showed that the deposited films are amorphous, and that there is no difference between the shape of the spectra of different microspheres and the waveguide, indicating that the coating procedure is reproducible.

Glass coated microspheres – AFM

Two quantities were measured:

-The surface roughness

-The number of defects/μm²

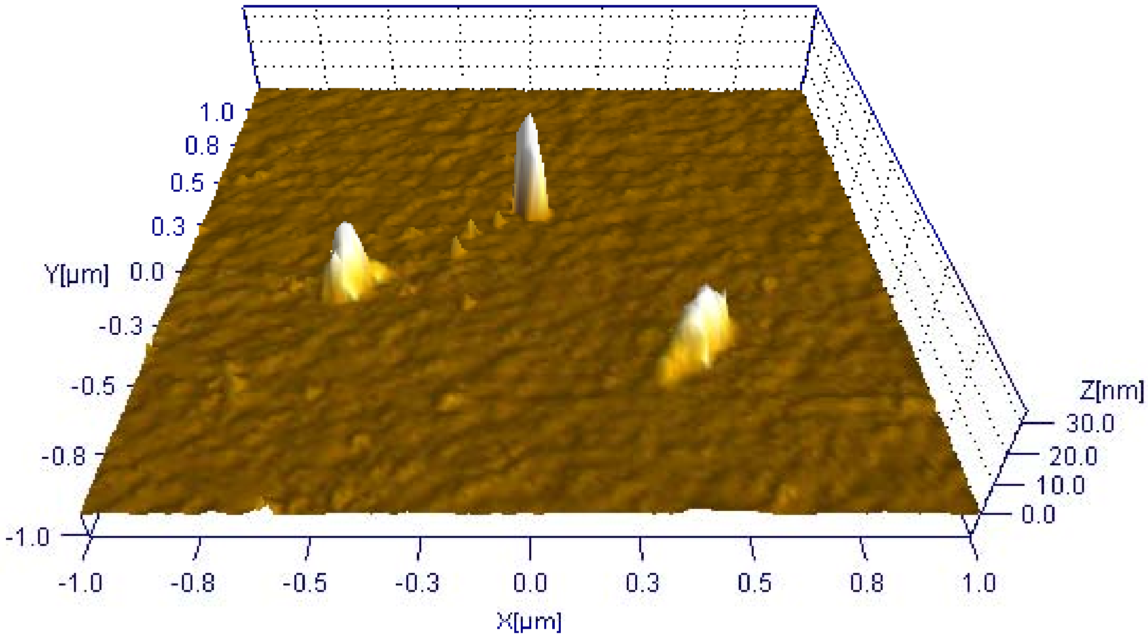

Glass coated microspheres – Defects

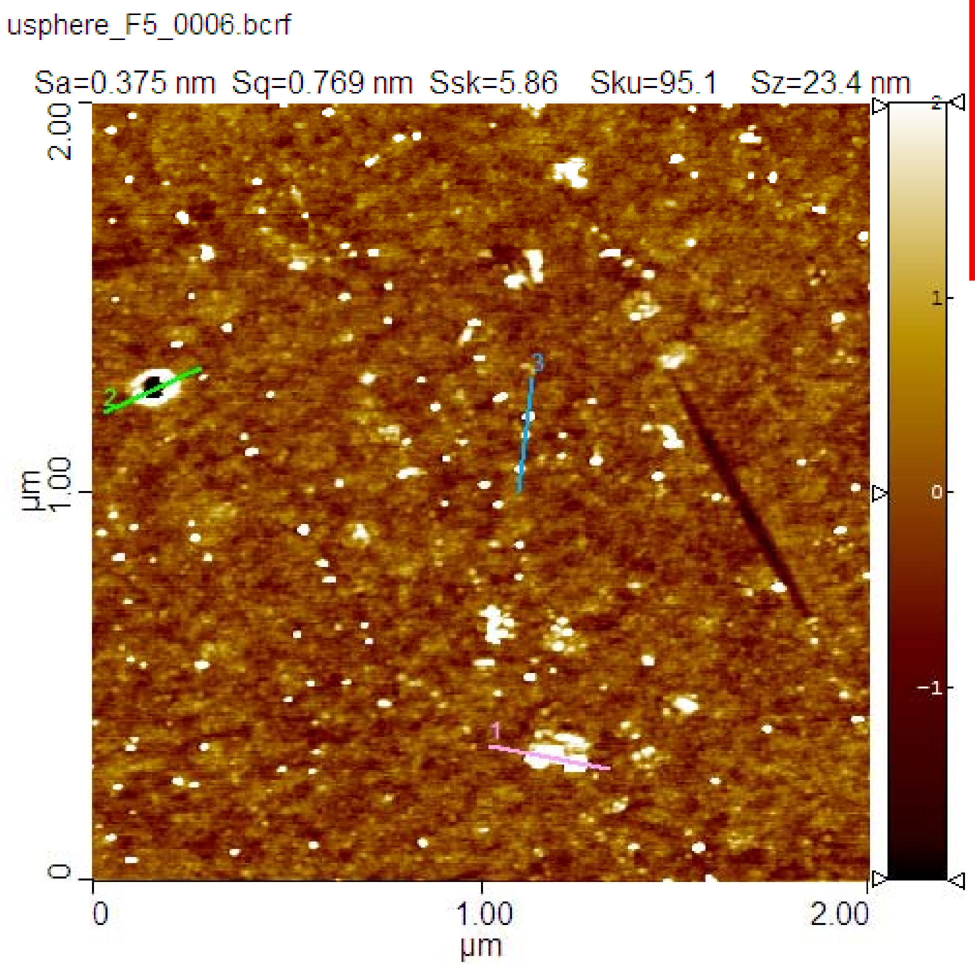

Defect types

- small defects (around 5 nm in height)
- Big defects (>15 nm in height)
- Holes (10 nm in depth)

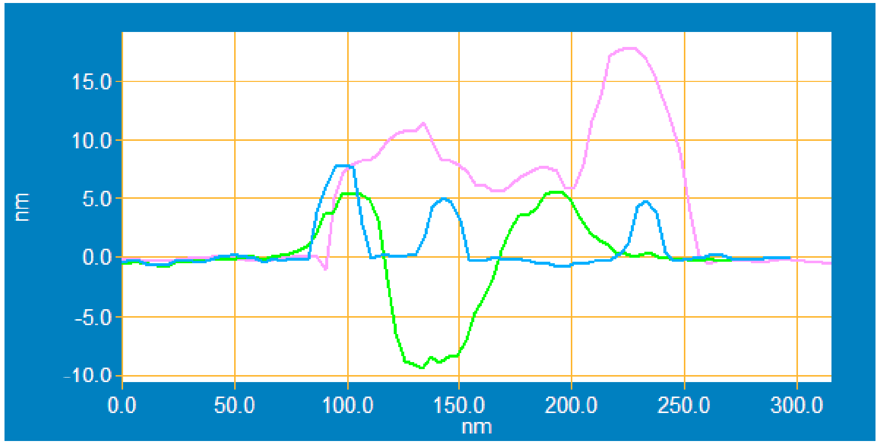

A low number of defects is needed to achieve high Q-factors

Glass coated microspheres – Roughness

For the surface roughness measurements the areas with no defects were chosen

Uncoated

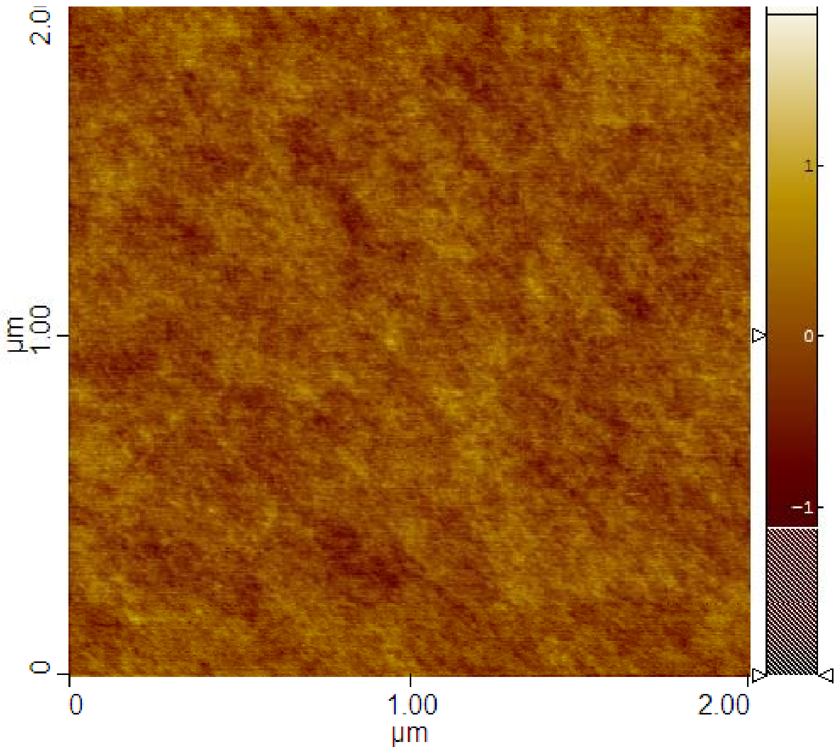

Coated

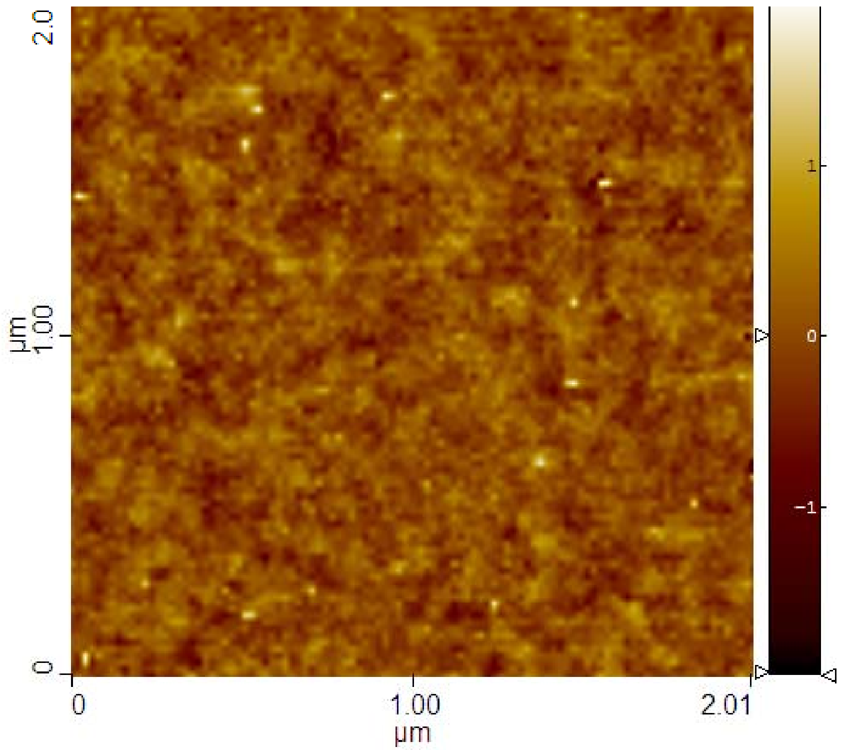

Glass coated microspheres – Surface assessment

Roughness calculated on 2x2 μm^2 areas

Defects counted on a

- 20x20μm^2 image
- 10x7μm^2 image

A 4th order bidimensional subtraction plus an histogram line-by-line levelling has been applied before computing the roughness

Defect density definition: (objects with Z_{max}>2 nm) numb./μm^2

Microsphere F5	Average absolute value surface roughness [nm]	Root mean square surface roughness [nm]	Defect density [numb./μm^2]
Uncoated	0.191 ± 0.004	0.242 ± 0.006	2.00 x10^{-2}
Coated	0.29 ±0.04	0.48 ± 0.19	6.24

Glass coated microspheres – Near Field

Effect of the coating thickness on the coupling efficiency

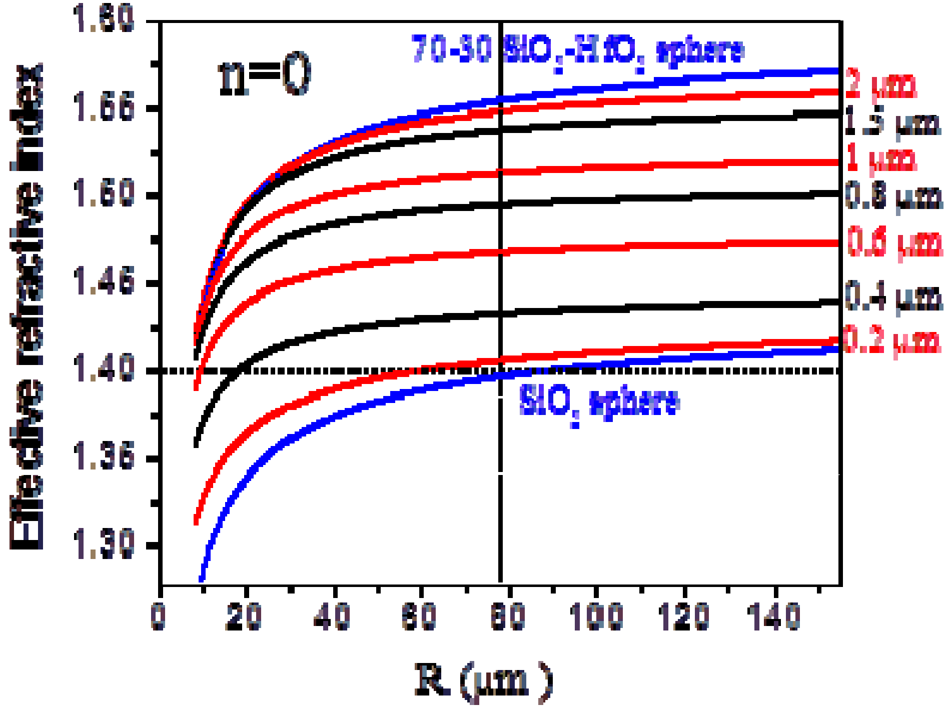

The effective refractive index of the $70SiO_2$-$30HfO_2$ coated microsphere as a function of the radius of the silica sphere for the fundamental equatorial (*n=0*; *l*-|*m*|=*0*) TE mode at 1560 nm. The refractive index of the sphere is 1.44 and of the coating 1.6. The coating thicknesses, given in µm, are also reported in the figure. The blue lines correspond to the border cases of no coating (blank sphere) or of very thick coating (bulk sphere with n=1.6). The horizontal dashed line corresponds to the effective refractive index of the propagation mode of a silica fiber taper with a waist of 3 µm. The vertical dashed line correspond to a silica sphere diameter of 155 µm which is the diameter of the sphere coated in our experiment.

Optics Express, 21 (2013) pp 20954-20963 "About the role of phase matching between a coated microsphere and a tapered fiber: experimental study "

Glass coated microspheres – Near Field

Effect of the coating thickness on the coupling efficiency

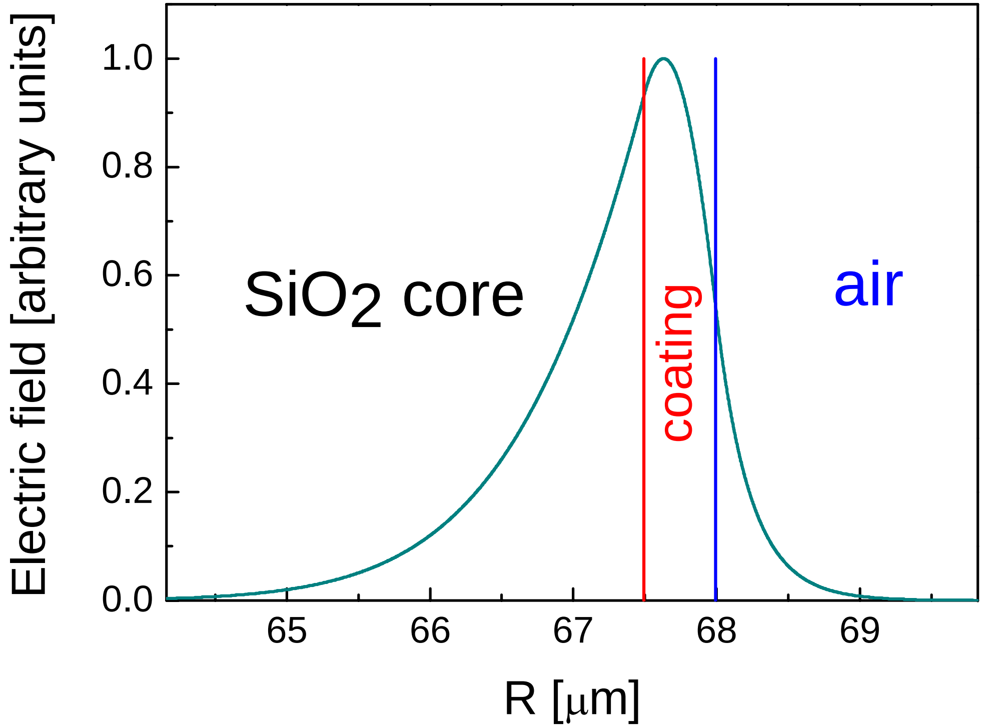

R= 68 μm

d= 0.5 μm

l = 400

N = 0

We need:

- high amount of E. field in the coating
- a reasonably long evanescent tail

d [μm]	*l*	R [μm]	E (sphere)	E (coating)	E (air)
0.2	388	68.0056	0.88637	0.05826	0.05537
0.3	391	68.0616	0.79013	0.13292	0.07695
0.5	400	67.9925	0.55117	0.3473	0.10153
0.7	409	67.996	0.38182	0.52335	0.09483
1	418	67.9822	0.23697	0.68933	0.07371
1.3	423	67.9418	0.15764	0.78497	0.05738

Glass coated microspheres – Laser WGMs

Effect of the coating thickness on the coupling efficiency

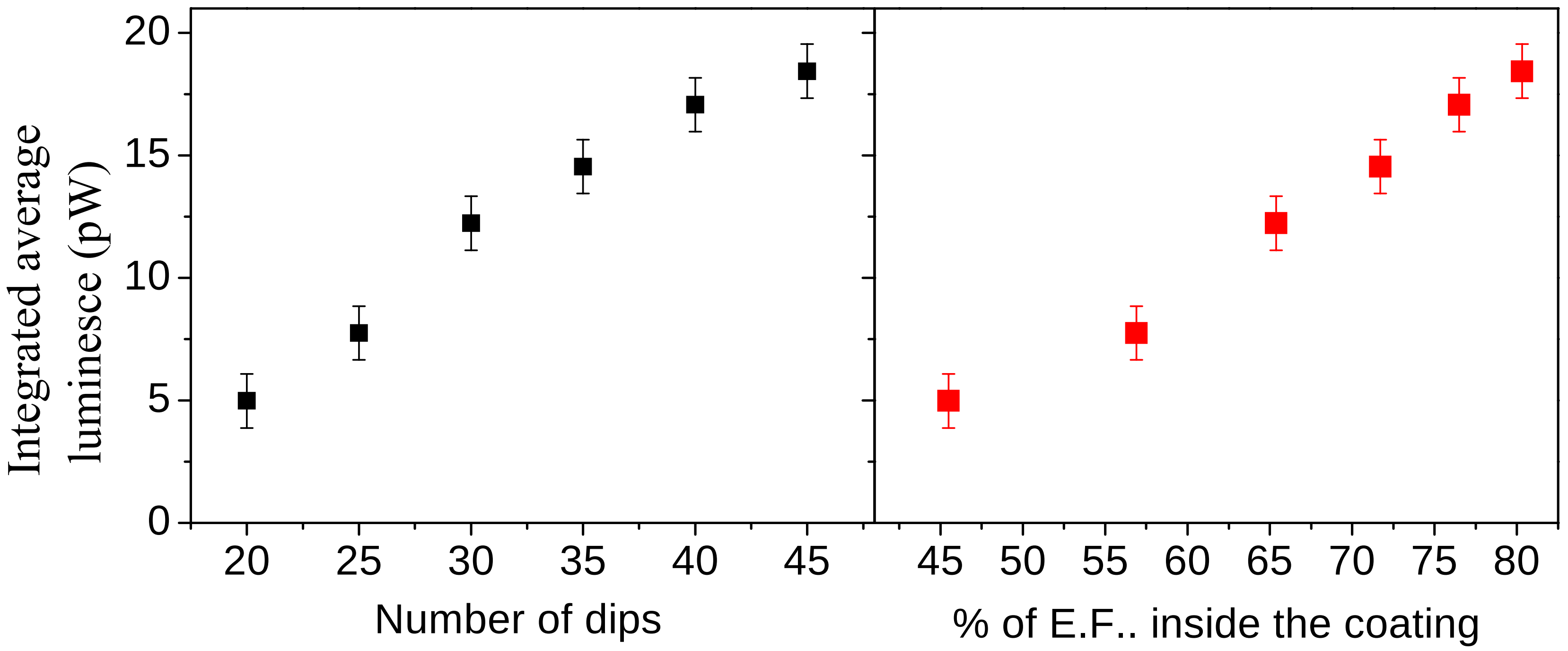

The average integrated luminescence in the 1535-1585 nm range for the 0.3 mol% Er^{3+} $70SiO_2$-$30HfO_2$ coated sphere in respect to the number of dips and to the percentage of the fundamental WGM electric field (e. f.) inside the coating as calculated from the number of dips.

Glass coated microspheres – Near Field

- The effect of the coating on the whispering gallery modes was studied
- The coating used was 70 % SiO_2 – 30% HfO_2 doped with 0.3 mol % Er^{3+}
- The spheres (D=140±10 μm) were characterized using a tapered fiber

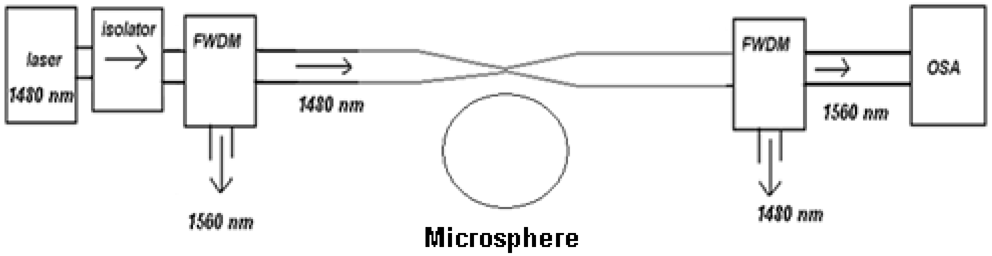

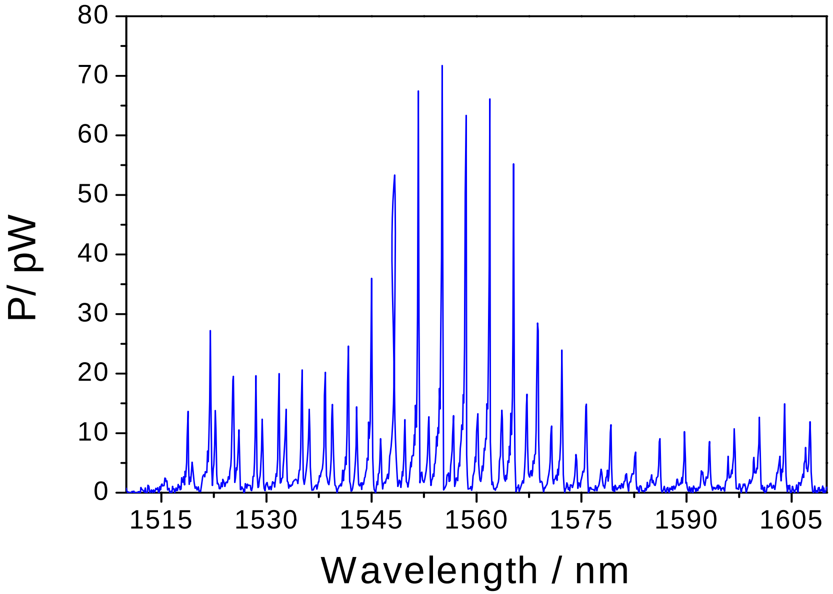

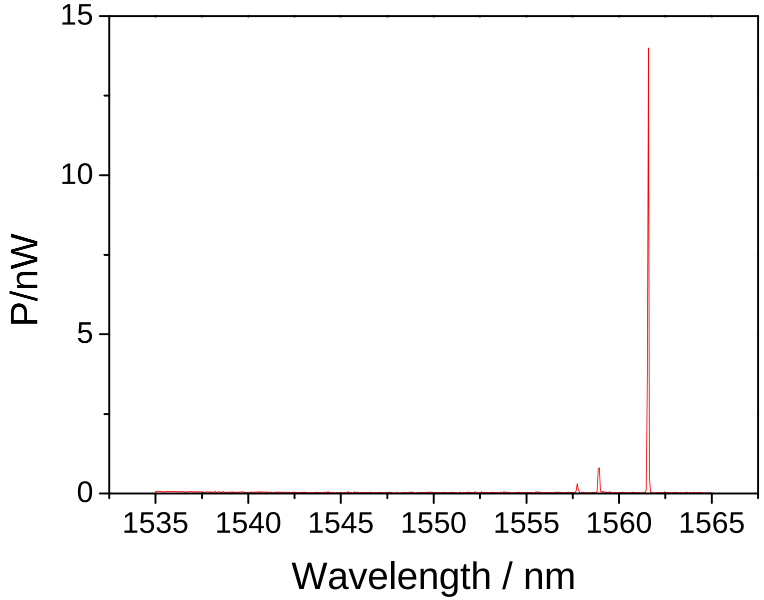

Glass coated microspheres – Laser WGMs

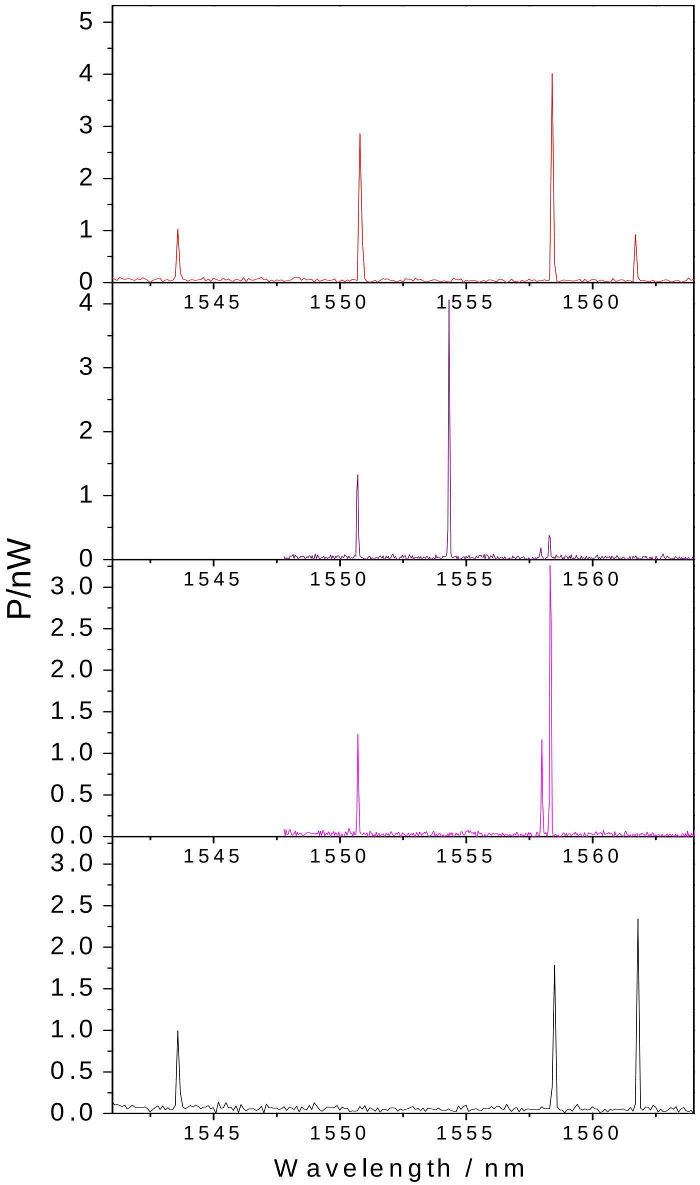

Excitation at 1.48 μm

Laser power: ≈ 120 mW.

The peak power of the detected modes was always in the range of nanowatts, the highest power detected being 30 nW.

WGM modes are clearly visible

Different modes are excited depending on the position of the taper

$$FSR_{l,l\pm1} = \frac{\lambda^2}{\pi N d}$$

N=1.6

λ = 1550 nm (wavelength of the signal)

FSR is 3.7 nm corresponding to a microsphere of about 130 μm

Q-factor is greater than the resolution of our detector (>3x10^4)

Thermal effects of coatings

Another important application of transparent coatings onto spherical microresonators concerns the possibility of reducing the thermal shift of the WGM resonances due to microsphere heating by the dissipated pump energy.

Actually, the shift is due both to the temperature-induced change in the refractive index (the thermo-optic coefficient) and to the temperature-induced increase of the diameter of the sphere (coefficient of thermal expansion)

Alessandro Chiasera, Yannik Dumeige, Patrice Féron, Maurizio Ferrari, Yoann Jestin, Gualtiero Nunzi Conti, Stefano Pelli, Silvia Soria, and Giancarlo C. Righini.“Spherical whispering-gallery-mode microresonators”Laser & Photonics Reviews 4 (2010) pp. 457-482

Thermal effects of coatings

$$\frac{1}{\lambda}\frac{\mathrm{d}\lambda}{\mathrm{d}T} = \alpha + \frac{1}{N}\frac{\mathrm{d}N}{\mathrm{d}T},$$

λ is the WGM wavelength

T is the temperature

α is the thermal-expansion coefficient

N is the refractive index of the microsphere

One can also take advantage of this characteristic of the spherical WGMRs to accurately measure the thermo-optic coefficient of the material of which the microresonator is made

Alessandro Chiasera, Yannik Dumeige, Patrice Féron, Maurizio Ferrari, Yoann Jestin, Gualtiero Nunzi Conti, Stefano Pelli, Silvia Soria, and Giancarlo C. Righini."Spherical whispering-gallery-mode microresonators"Laser & Photonics Reviews 4 (2010) pp. 457-482

Thermal effects of coatings

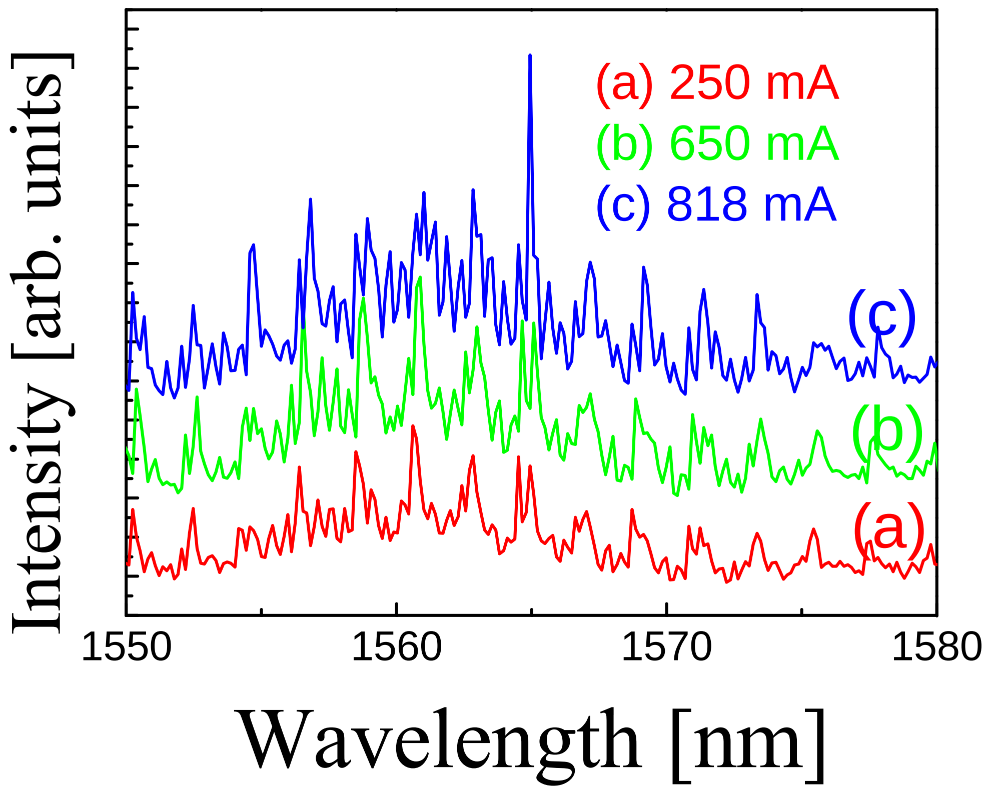

Whispering gallery modes emission spectra of a silica microsphere of 250 μm in diameter and coated by a film of $70SiO_2$-$30HfO_2$ activated with 1 mol% Er^{3+}. The thickness of the coating is 0.8 μm. Spectra are obtained at different current of the 1480 nm pump laser.

No red shift increasing pump power

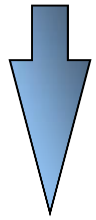

due to the silica-hafnia coating

Alessandro Chiasera, Yannik Dumeige, Patrice Féron, Maurizio Ferrari, Yoann Jestin, Gualtiero Nunzi Conti, Stefano Pelli, Silvia Soria, and Giancarlo C. Righini.“Spherical whispering-gallery-mode microresonators”Laser & Photonics Reviews 4 (2010) pp. 457-482

Conclusions and Perspectives

- Photonic crystals that exhibit specific morphologic, structural, and optical properties allow to develop interesting new physical concepts, as well as novel photonic devices based on the control of the light.

- RF – sputtering and colloidal route are complementary techniques suitable for fabrication of high Q 1-D photonic microcavities and versatile 3-D photonic opals activated by rare earth ions, respectively.

- WGMs laser or frequency combs can be tailored by suitable coating of spherical microresonators

ACKNOWLEDGEMENTS:

- **CNES SHYRO project (2011-2015)**
- **NSBMO research project (2010-2013)**
- **Polish Ministry of Science and Higher Education "Mobility Plus" Program**
- **SiMeCro research project (2012-2013) Caritro Foundation**
- **MAE Significant Bilateral Project between Italy and Egypt titled "Smart optical nanostructures for green photonics (2013-2015)**

Welcome to
CIMTEC 2014

Montecatini Terme, Italy - June 9-20, 2014
13th International Ceramics Congress (June 9-13, 2014)
&
6th Forum on New Materials (June 16-20, 2014)

Symposium CL
Inorganic Materials Systems for Optical and Photonic Applications

XVIth International Krutyn Summer School 2014, Krutyń, Masurian Lake District, Poland, August 31-September 6, 2014

http://glassphotonics.ikss.eu/

Lanthanide-based photonic materials and structures: breakthrough applications and cutting edge systems